A Tsunami Forecast Model for Chignik, Alaska

Dylan Righi

Contents

Abstract

1.0 Background and Objectives

2.0 Forecast Methodology

3.0 Model Development

- 3.1 Forecast Area
- 3.2 Historical Events and Data
- 3.3 Model Setup

4.0 Results and Discussion

- 4.1 Model Validation
- 4.2 Model Stability

5.0 Summary and Conclusion

6.0 Acknowledgments

7.0 References

Figures

Appendix A - *.in file

Appendix B – Propagation Database Unit Sources

Abstract

In support of the National Oceanic and Atmospheric Administration's tsunami forecast system, we have developed and tested a numerical tsunami model for the community of Chignik, Alaska. The Chignik tsunami forecast model employs the optimized version of the Method of Splitting Tsunami (MOST) numerical code and has been validated and tested using data from 12 historical tsunamis and a set of 19 synthetically generated mega events (forced by Mw 9.3 earthquakes). A high-resolution reference model, without limitations on computational run-times, has also been developed to provide comparison for the forecast model. Validation results show good agreement between the forecast and reference models. The forecast model developed is seen to be stable under forcing from both large and small modeled tsunami events and will provide dependable warnings in the event of a tsunami that might threaten the residents and structures of Chignik.

1.0 Background and Objectives

The National Oceanic and Atmospheric Administration (NOAA) Center for Tsunami, Research (NCTR) at the NOAA Pacific Marine Environmental Laboratory (PMEL) has developed a tsunami forecasting capability for operational use by NOAA's two Tsunami Warning Centers located in Hawaii and Alaska (Titov *et al.*, 2005). The system is designed to efficiently provide basin-wide warning of approaching tsunami waves accurately and quickly. The system, termed Short-term Inundation Forecast of Tsunamis (SIFT), combines real-time tsunami event data with numerical models to produce estimates of tsunami wave arrival times and amplitudes at a coastal community of interest. The SIFT system integrates several key components: deep-ocean observations of tsunamis in real time, a basin-wide pre-computed propagation database of water level and flow velocities based on potential seismic unit sources, an inversion algorithm to refine the tsunami source based on deep-ocean observations during an event, and high-resolution tsunami forecast models.

Chignik is located on the rugged south side of the Alaskan Peninsula, about midway between

Kodiak and Dutch Harbor, Alaska. Anchorage, Alaska is 730 kilometers to the northwest. Chignik sits on Anchorage Bay, a small bay that in turn opens to Chignik Bay and then the North Pacific. The current population is 91 (2010 US Census), living in 41 of the 105 housing units in the community. Commercial fishing is the main economic activity in the community, and a fish processing and canning facility are located there. Due to this, the population in the summer months increases significantly. Chignik can be reached by airplane or boat. There is a gravel runway located to the northeast of the town, also on Anchorage Bay, with regular flights from King Salmon. The Alaskan Marine Highway System ferry docks in Chignik, providing transport to Kodiak twice a month. In Figure 1, a photograph taken from the hills above the town, the main docks and the fish processing plants can be seen.

This goal of this work is to provide a high quality forecast model that will enable emergency planners at the local, state and national levels to protect the people and resources of Chignik Bay from the dangers of tsunami events.

2.0 Forecast Methodology

A high-resolution inundation model was used as the basis for development of a tsunami forecast model to operationally provide an estimate of wave arrival time, wave height, and inundation Chignik following tsunami generation. All tsunami forecast models are run in real time while a tsunami is propagating across the open ocean. The Chignik model was designed and tested to perform under stringent time constraints given that time is generally the single limiting factor in saving lives and property. The goal of this work is to maximize the length of time that residents of the area have to react to a tsunami threat by providing accurate information quickly to emergency managers and other officials responsible for the community and infrastructure.

The general tsunami forecast model, based on the Method of Splitting Tsunami (MOST), is used in the tsunami inundation and forecasting system to provide real-time tsunami forecasts at selected coastal communities. The model runs in minutes while employing high-resolution grids constructed by the National Geophysical Data Center. The Method of Splitting Tsunami (MOST) is a suite of numerical simulation codes capable of simulating three processes of

tsunami evolution: earthquake, transoceanic propagation, and inundation of dry land. The MOST model has been extensively tested against a number of laboratory experiments and benchmarks (Synolakis *et al.*, 2008) and was successfully used for simulations of many historical tsunami events. The main objective of a forecast model is to provide an accurate, yet rapid, estimate of wave arrival time, wave height, and inundation in the minutes following a tsunami event. Titov and González (1997) describe the technical aspects of forecast model development, stability, testing, and robustness, and Tang *et al.*, 2009 provide detailed forecast methodology

A basin-wide database of pre-computed water elevations and flow velocities for unit sources covering worldwide subduction zones has been generated to expedite forecasts (Gica *et al.*, 2008). As the tsunami wave propagates across the ocean and successively reaches tsunameter observation sites, recorded sea level is ingested into the tsunami forecast application in near real-time and incorporated into an inversion algorithm to produce an improved estimate of the tsunami source. A linear combination of the pre-computed database is then performed based on this tsunami source, now reflecting the transfer of energy to the fluid body, to produce synthetic boundary conditions of water elevation and flow velocities to initiate the forecast model computation.

Accurate forecasting of the tsunami impact on a coastal community largely relies on the accuracies of bathymetry and topography and the numerical computation. The high spatial and temporal grid resolution necessary for modeling accuracy poses a challenge in the run-time requirement for real-time forecasts. Each forecast model consists of three nested grids with increasing spatial resolution in the finest grid, and temporal resolution for simulation of wave inundation onto dry land. The forecast model utilizes the most recent bathymetry and topography available to reproduce the correct wave dynamics during the inundation computation. Forecast models, including the Chignik model, are constructed for at-risk populous coastal communities in the Pacific and Atlantic Oceans. Previous and present development of forecast models in the Pacific (Titov *et al.*, 2005; Titov, 2009; Tang *et al.*, 2009; Wei *et al.*, 2008) have validated the accuracy and efficiency of each forecast model currently implemented in the real-time tsunami forecast system. Models are tested when the opportunity

arises and are also used for scientific research. Tang *et al.*, 2009 provide forecast methodology details.

3.0 Model Development

The general methodology for modeling at-risk coastal communities is to develop a set of three nested grids, referred to as A, B, and C-grids, each of which becomes successively finer in resolution as they telescope into the population and economic center of the community of interest. The offshore area is covered by the largest and lowest resolution A-grid while the near-shore details are resolved within the finest scale C-grid to the point that tide gauge observations recorded during historical tsunamis are resolved within expected accuracy limits. The procedure is to begin development with large spatial extent merged bathymetric topographic grids at high resolution, and then optimize these grids by sub-sampling to coarsen the resolution and shrink the overall grid dimensions to achieve a 4 to 10 hr simulation of modeled tsunami waves within the required time period of 10 min of wall-clock time. The basis for these grids is a high-resolution digital elevation model constructed by the National Geophysical Data Center and NCTR using all available bathymetric, topographic, and shoreline data to reproduce the wave dynamics during the inundation computation for an at-risk community. For each community, data are compiled from a variety of sources to produce a digital elevation model referenced to Mean High Water in the vertical and to the World Geodetic System 1984 in the horizontal (http://ngdc.noaa.gov/mgg/inundation/tsunami/inundation.html). From these digital elevation models, a set of three high-resolution, "reference" elevation grids are constructed for development of a high-resolution reference model from which an 'optimized' model is constructed to run in an operationally specified period of time. The operationally developed model is referred to as the optimized tsunami forecast model or forecast model for brevity.

Development of an optimized tsunami forecast model for Chignik began with the spatial extent merged bathymetric/topographic grids provided by the NGDC shown in Figure 2. Grid dimension extension and additional information were updated as needed and appropriate. A significant portion of the modeled tsunami waves, typically 4 to 10 hr of modeled tsunami time, pass through the model domain without appreciable signal degradation. Table 1 provides

specific details of both reference and tsunami forecast model grids, including extents and complete input parameter information for the model runs is provided in Appendix A.

3.1 Forecast Area

Chignik and Anchorage Bay are shown in the satellite image presented in Figure 3. Anchorage Bay opens to the north-west to Chignik Bay and has an opening of 1.7 kms and is almost 3 kilometers lengthwise. Chignik Airport is located on the eastern side of the Bay, and the under-construction small boat harbor can be seen just south of the airstrip. It has since been completed and presented issues during the development of the model grids, as will be discussed in Section 3.3 later. The community of Chignik itself is centered at the south edge of Anchorage Bay on the level area at the foot of the hills surrounding the bay. A significant portion of the area is low-lying wetlands, drained by Indian Creek. Figure 4 shows the cannery and other industrial buildings near the main dock and the low wetlands surrounding. Most of the residences are behind the cannery away from the beach, and to the west near Indian Creek. The beach in front of town is narrow, with a steep profile as seen in the image in Figure 5.

The area around Chignik on a larger scale is fairly complicated. Anchorage Bay, as mentioned above, opens to the larger Chignik Bay, which is on the order of 20 kilometers across. Just to the northwest of Anchorage Bay is the long, thin Mud Bay, which is very shallow and protected at its mouth by a barricade island. Next to the northwest is Chignik Lagoon, a much larger bay where the community of Chignik Lagoon sits. Chignik Lagoon is also a shallow, protected bay and is not seen to be threatened by tsunami wave heights in our modeling.

On a larger scale, Chignik Bay opens to the southeast to the northern Pacific Ocean. Kodiak Island is 280 kilometers to the northeast. The bathymetry to the south is varied, with depth of hundreds of meters on the shelf then dropping to 5000-6000 meters on the Pacific Ocean floor. Between these is the Aleutian Trench, with depths of up to 8000 meters, marking the boundary between the Pacific and North American tectonic

plates. The nearness of this boundary stresses the importance of developing an accurate and reliable tsunami forecast model for Chignik to protect its population.

3.2 Historical Events and Data

The community of Chignik does not have a dedicated tide gauge. The closest tide gauge to Chignik is situated in Sandpoint, Alaska and is not near enough to be of use for model validation. Historical accounts of tsunami run-up heights are, however, available from the National Geophysical and Data Center tsunami run-up database (http://www.ngdc.noaa.gov/nndc/struts/form?t=101650&s=167&d=166) for the 1946 Unimak and 1964 Alaska events. As discussed later in this report, these events are used for model validation and the run-up data is used to compare the model results. A warning-point location consistent with these available historical data was selected. The location of the Chignik warning point for development of the tsunami forecast model is shown in Figure 6. The absolute location of this warning point is 56.2961°N, 158.4022°W. The depth of this point in the forecast model is 7.93 meters.

3.3 Model Setup

The grids developed for the reference and forecast models were derived from the Pacific basin-wide 30 arc-second grid developed at NCTR, and the 1 second and 1/3 arc-second digital elevation models (DEMs) developed by NGDC (Taylor *et al*, 2008). Perspective views of these DEMs are shown in Figure 2. The Chignik 1 second grid covers from 159.2601 to 157.5599 °W and 55.7899 to 56.7201 °N, and has a resolution of 17 and 31 meters in the X and Y directions. The 1/3 second grid covers the smaller extent of 158.54 to 158.21 °W and 56.23 to 56.49 °N, with resolutions of 5.7 and 10 meters.

The grid extents and parameters of the forecast and reference model grids are detailed in Table 1. The forecast and reference grid sets were set up using matching boundaries. The A-grids cover the Alaskan Peninsula from Unimak Island at the west edge to Kodiak Island to the east.

The extent of the A-grids to the south is designed to extend past the Aleutian Trench. The B-grids focus on the region of Chignik Bay and the complicated coastline to the south.
The highest resolution C-grids zoom in on Anchorage Bay and Chignik itself, with the goal describing the waves and water levels of the Bay and inundation at the coast. The developed reference and forecast model grids are shown in Figures 6 and 7, respectively.

Once initial testing of the grids began, high-frequency instabilities were seen in the grids near the coast of the B and C grids. This was removed by applying a 5-point Hanning filter to the entire grid domain to smooth points. Another issue that needed to be dealt with was Chignik's small boat harbor. The NGDC DEMs provided show the bathymetry of the small boat harbor as it was being constructed, and includes two construction dykes across the main body of the small boat harbor (as seen in Figure 12 of Taylor et. al.). Further investigation shows that the dredging work had been completed and these dykes are no longer present. The bathymetry of the forecast and reference C-grids was hand edited to reflect these changes. This is important, as tsunami driven high flow velocities in small boat harbors are often the cause of high damage values from tsunami events.

4.0 Results and Discussion

The developed models are tested for accuracy and stability using a combination of historical and synthetic tsunami events. The goal is to compare the fast-running forecast model to the high-resolution reference model and check that important detail or dynamics was not lost in the sub-sampling process of developing the forecast model. Also, to check that the forecast model is able to supply quality wave height estimates under strong forcing, a large set of synthetic mega-tsunami events is used to test model stability.

4.1 Model Validation

We use twelve historical tsunamis to validate and test the Chignik forecast and reference models. The locations, magnitudes, and unit source combinations used to describe these events are described in Table 2. The events selected for testing range from smaller to larger

originating earthquakes (7.7 to 9.2 M_W), and are from varied locations around the Pacific Rim. The majority of the events are more recent since we have higher quality descriptions of the earthquakes and can describe the tsunamagenic response more accurately. The locations and magnitudes of the eleven historical events are plotted in Figure 8.

Results and comparisons from the forecast and reference models for the historical events are shown in Figures 9 - 20. In each figure the top two axes show the maximum amplitude for the forecast and reference models, respectively, and the lower axis shows the time series of wave amplitude from both models at the location of the chosen Chignik warning point (whose location is shown in Figure 7). Note that the color scale and axes limits change from figure to figure.

The 1946 Unimak 8.5 M_W earthquake is the first historical event used for validation. Figure 9 shows the forecast and reference model results. Outside of Anchorage Bay the model show similar patterns and values, while inside the bay the forecast model predicts a maximum wave height on the order of 30 centimeters while the reference model shows slightly higher values. The time-series at the warning point are well matched with the more obvious departure coming with the third wave of the reference model being higher than the forecast model. Eyewitness reports from Chignik for this event are available (NOAA Tsunami Runup Database, http:// http://www.ngdc.noaa.gov/nndc/struts/form?t=101650&s=167&d=166) and suggest that a 1.52 meter wave was observed, which is much larger than predicted values of 0.4 and 0.3 meters in the reference and forecast models.

The next two events predicted are the largest earthquakes recorded: the 1960 Chilean and 1964 Alaskan earthquakes. As seen in Figures 10 and 11, the tsunami forecast and reference models predict close to 3 meter waves at Chignik for both of these events. Both lead to strong inundation of the low wetlands area in Chignik. The time series show results from the forecast and reference models matching well. Eyewitness data from the 1964 Alaska tsunami at Chignik reported a maximum wave height of 3 meters, matching the model predictions well.

The next eight historical events presented Figures 12 – 19) do not present a threat to Chignik and Anchorage Bay. They models predict maximum wave heights only on the order of 10 centimeters in the C-grids. For all these cases tested, it is important to note that the forecast model is able to predict results that closely follow those from the higher resolution reference model. The last historical event presented here for model validation is the one caused by the Chilean earthquake of 2010, which caused major destruction and over 500 deaths in Chile. The forecast and reference models shown in Figure 20 show matching patterns, with wave height maxima increasing into Anchorage Bay. The forecast model shows, as seen in other results, slightly lower heights than the reference model. Looking at the time series in the lower panel show the models to match well, both in wave arrival time and height. The Chilean tsunami is not predicted to lead to any inundation in Chignik.

4.2 Model stability testing using synthetic scenarios

To further test the stability and robustness of the forecast model, we use a set of 21 synthetic tsunamis. These events are 'synthetic' in the sense that they do not represent actual historical earthquakes, but allow us the flexibility to stress test our model using large forcing inputs from many different directions. Of these, 19 are Mw 9.3 events that each use a set of 20 unit sources, corresponding to a rupture area of 1000 km by 100 km, and are located all around the Pacific Basin and in each subduction zone. For comparison, the 2004 Indian Ocean tsunami that resulted in hundreds of thousands of deaths in Indonesia, and was detectable globally was the result of a Mw 9.1 earthquake. We also run tests using a medium Mw 7.5 and a micro-event, to make sure the model triggers correctly for low energy events. Table 3 describes the synthetic events used and their unit source combinations and Figure 21 shows the locations of these events and their positions relative to Chignik. The resulting maximum wave amplitude and time series of wave amplitude at the Chignik warning point as predicted from the forecast model are shown in Figures 22 - 42.

The largest tsunami wave at Chignik predicted from these results is due to the ACSZ 22-31 mega-event. This event, the closest of the mega-events tested, is centered on the Aleutian subduction zone to the southwest of Chignik. The maximum wave heights, shown in the upper panel of Figure 28 are a devastating 20 meters high over most of Anchorage Bay and Chignik. The initial wave, seen in the time-series at the warning point, is greater than 5 meter drop in height followed by a first wave of 20 meters. Subsequent waves are smaller, but still on the order of 5-10 meters. The initial positive wave hits the community almost 2 hours after the event; so one would hope that in this case warnings and evacuations would save lives.

In the other synthetic cases presented, there are significant wave heights predicted and some inundation. The 4 events (Figures 22 – 25) from the Kamchatka-Kuril-Japan-Izu-Mariana-Yap zone (KISZ), on the northwestern boundary of the Pacific, cause wave heights on the order of one meter at Chignik and minimal inundation along the creek and wetland areas. The nearer events from the Aleutian-Alaska-Cascadia subduction zone shown in Figures 26 – 30 cause the most significant waves, as would be expected. The closest ACSZ event has already been discussed, but for the other, farther away events on the ACSZ subduction zone wave heights from 1-2 meters are predicted. The Central and South America sources (CSSZ) lead to 0.5 –2 meter wave height response at Chignik (Figures 31 – 34). Interestingly, the farthest away of these, CSSZ 102-111, causes the larger wave heights due to the directions the wave energy is focused. Almost all of the events from sources in the southeast Pacific Ocean shown in Figures 35 – 40 cause significant 1 – 2 meter waves at Chignik. The strongest of these are from the New Zealand-Kermadec-Tonga (NTSZ) and New Britain-Solomons-Vanuatu (NVSZ) zones. Lastly, the medium and micro synthetic events (Figures 41 and 42) show minimal and negligible response at Chignik. This result is still important in that is shows that the forecast model will correctly trigger and predict events with very low energy.

5.0 Summary and Conclusions

We have developed a set of optimized and reference tsunami forecast models for Chignik, Alaska. The models have been validated using historical tsunamis events and stress-tested using synthetic mega-tsunami events. For historical events the high-resolution reference model and the operational forecast model predictions show very good agreement in predicting arrival times and magnitudes of tsunami waves. Synthetic tsunami event testing suggests that largest threat for Chignik comes from earthquakes in the Aleutian-Alaska-Cascadia subduction and the Kamchatka-Kuril-Japan-Izu-Mariana-Yap zones. The grid developed for the forecast model has resolutions in longitude and latitude of 2.0 and 1.0 arc-seconds – corresponding to a grid spacing of approximately 34 meters. Four hours of model time can be run in under 10 minutes, providing fast wave height estimates.

The models give accurate predictions of wave height and water velocity in response to tsunami forcing. These models are part of NOAA's tsunami forecast and warning system and will be used to predict, in real-time, the potential threat of tsunami waves for the people and resources of the community of Chignik.

6.0 Acknowledgments

The author wishes to thank Yong Wei, Burak Uslu and Diego Arcas for guidance and assistance with model development and troubleshooting, Lijuan Tang for providing source information for two of the historical events, Edison Gica and Michael Spillane for helpful document feedback, Nazila Merati for model testing, and Marie Eble and Lindsey Wright for editorial review and management.

7.0 References

Gica, E., M. Spillane, V.V. Titov, C. Chamberlin, and J.C. Newman (2008): Development of the forecast propagation database for NOAA's Short-term Inundation Forecast for Tsunamis (SIFT). NOAA Tech. Memo. OAR PMEL-139, 89 pp.

Synolakis, C.E., E.N. Bernard, V.V. Titov, U.Kanoglu and F. Gonzalez (2008). Validation and verification of tsunami numerical models. *Pure Appl. Geophys.*, *165*(11–12), 2197–2228.

Tang, L., V. V. Titov, and C. D. Chamberlin (2009), Development, testing, and applications of site-specific tsunami inundation models for real-time forecasting, J. Geophys. Res., 114, C12025, doi:10.1029/2009JC005476.

Tang, L.J., Chamberlin, C., Titov, V.V. and Tolkova, E. (2006): A Stand-by Inundation Model f Kahului, Hawaii for NOAA Short-term Inundation Forecasting For Tsunamis (SIFT). NOAA Tech. Memo. OAR PMEL-XXX, 56p.

Taylor, L.A., B.W. Eakins, P.R. Medley, K.S. Carignan, R.R. Warnken and E. Lim (2008): Digital elevation models of Chignik, Alaska: Procedures, data sources and analysis. NOAA Technical Memorandum NESDIS NGDC-27, October 2008, 26 pp.

Titov, V.V. (2009): Tsunami forecasting. Chapter 12 in *The Sea, Volume 15: Tsunamis*, Harvard University Press, Cambridge, MA and London, England, 371–400.

Titov, V.V., Gonzalez, F.I., Bernard, E.N., Eble, M.C., Mofjeld, H.O., Newman, J.C. and Venturato, A.J. (2005). Real-time tsunami forecasting: challenges and solutions. Natural Hazards, 35(1), 41-58.

Titov, V.V., H.O. Mofjeld, F.I. Gonzalez and J.C. Newman (1999): Offshore forecasting of Alaska-Aleutian subduction zone tsunamis in Hawaii. NOAA Technical Memorandum. ERL PMEL-114, January 1999, 22 pp.

Wei, Y, E. N. Bernard, L. Tang, R. Weiss, V.V. Titov, C. Moore, M. Spillane, M. Hopkins and U. Kanoglu (2008): Real-time experimental forecast of the Peruvian tsunami of August 2007 for U.S. coastlines. *Geophys. Res. Lett.*, *35*, L04609, doi: 10.1029/2007GL032250.

Tables

Grid	Region	Reference Model				Forecast Model			
		Coverage Lat. [ºN] Lon. [ºE]	Cell Size ["]	nx x ny	Time Step [sec]	Coverage Lat. [º N] Lon. [ºE]	Cell Size ["]	nx x ny	Time Step [sec]
A	Alaska	53.8175 – 57.9597 198.254 – 205.4807	48 x 32	543 x 467	3.0	53.8197 – 57.9597 198.254 – 205.4840	108 x 72	242 x 208	4.8
B	Alaskan Penisula	55.87 – 56.52 201.27 – 202.2189	8 x 6	428 x 391	2.0	55.87 – 56.52 201.27 – 202.22	18 x 12	191 x 196	3.2
C	Chignik	56.29 – 56.38 201.54 – 201.67	0.67 x 0.33	710 x 983	0.25	56.29 – 56.38 201.54 – 201.67	2.0 x 1.0	235 x 325	0.8
Minimum offshore depth [m]				5				5	
Water depth for dry land [m]				0.1				0.1	
Friction coefficient [n^2]				0.0009				0.0009	
CPU time for 4-hr simulation				4.5 hr				10.2 min	

Computations were performed on a single Intel Xeon E5670 processor at 2.93 GHz, Dell PowerEdge R510.

Table 1 MOST model setup of the reference and forecast models for Chignik, Alaska.

Earthquake / Seismic				Model		
Event	USGS Date Time (UTC) Epicenter	CMT Date Time (UTC) Centroid	Magnitude Mw	Tsunami Magnitude[1]	Subduction Zone	
1946 Unimak	01 Apr 12:28:56 52.75ºN 163.50ºW	01 Apr 12:28:56 53.32ºN 163.19ºW	[2]8.5	8.5	Aleutian-Alaska-Cascadia (ACSZ)	7 ł
1960 Chile	22 Apr 19:11:17 39.50ºS 74.50ºW		[3]9.2	9.5	Central-South America (CSSZ)	
1964 Alaska	28 Mar 03:36:00 [3]61.02ºN 147.65ºW	28 Mar 03:36:14 61.10ºN 147.50ºW	[3]9.2	9.0	Aleutian-Alaska-Cascadia (ACSZ)	7
1994 East Kuril	04 Oct 13:22:58 43.73ºN 147.321ºE	04 Oct 13:23:28.5 43.60ºN 147.63ºE	[5]8.3	8.1	Kamchatka-Kuril-Japan-Izu-Mariana-Yap (KISZ)	9
1996 Andreanov	10 Jun 04:03:35 51.56ºN 175.39ºW	10 Jun 04:04:03.4 51.10ºN 177.410ºW	[5]7.9	7.8	Aleutian-Alaska-Cascadia (ACSZ)	2
2003 Rat Island	17 Nov 06:43:07 51.13ºN 178.74ºE	17 Nov 06:43:31.0 51.14ºN 177.86ºE	[5]7.7	7.8	Aleutian-Alaska-Cascadia (ACSZ)	6
2006 Tonga	03 May 15:26:39 20.13ºS 174.161ºW	03 May 15:27:03.7 20.39ºS 173.47ºW	[5]8.0	8.0	New Zealand-Kermadec-Tonga (NTSZ)	6
2006 Kuril	15 Nov 11:14:16 46.607ºN 153.230ºE	15 Nov 11:15:08 46.71ºN 154.33ºE	[5]8.3	8.1	Kamchatka-Kuril-Japan-Izu-Mariana-Yap (KISZ)	6 1
2007 Kuril	13 Jan 04:23:20 46.272ºN 154.455ºE	13 Jan 04:23:48.1 46.17ºN 154.80ºE	[5]8.1	7.9	Kamchatka-Kuril-Japan-Izu-Mariana-Yap (KISZ)	-
2007 Solomon	01 Apr 20:39:56 8.481ºS 156.978ºE	01 Apr 20:40:38.9 7.76ºS 156.34ºE	[3]8.1	8.2	New Britain-Solomons-Vanuatu (NVSZ)	1
2009 Samoa	29 Sep 17:48:10 15.509ºS 172.034ºW	29 Sep 17:48:26.8 15.13ºS 171.97ºW	[5]8.1	8.1	New Zealand-Kermadec-Tonga (NTSZ)	6
2010 Chile	27 Feb 06:34:14 35.909ºS 72.733ºW	27 Feb 06:35:15.4 35.95ºS 73.15ºW	[5]8.8	8.8	Central-South America (CSSZ)	6 1 -

[1] Preliminary source – derived from source and deep-ocean observations

[2] López and Okal (2006)

[3] United States Geological Survey (USGS)

Table 2 Historical events used for validation of the Chignik, Alaska model.

Sce No.	Scenario Name	Source Zone	Tsunami Source	α (m)
		Mega-tsunami scenario		
1	KISZ 1-10	Kamchatka-Yap-Mariana-Izu-Bonin	A1-A10, B1-B10	25
2	KISZ 22-31	Kamchatka-Yap-Mariana-Izu-Bonin	A22-A31, B22-B31	25
3	KISZ 32-41	Kamchatka-Yap-Mariana-Izu-Bonin	A32-A41, B32-B41	25
4	KISZ 56-65	Kamchatka-Yap-Mariana-Izu-Bonin	A56-65, B56-65	25
5	ACSZ 6-15	Aleutian-Alaska-Cascadia	A6-A15, B6-B15	25
6	ACSZ 16-25	Aleutian-Alaska-Cascadia	A16-A25, B16-B25	25
7	ACSZ 22-31	Aleutian-Alaska-Cascadia	A22-A31, B22-B31	25
8	ACSZ 50-59	Aleutian-Alaska-Cascadia	A50-A59, B50-B59	25
9	ACSZ 56-65	Aleutian-Alaska-Cascadia	A56-A65, B56-B65	25
10	CSSZ 1-10	Central and South America	A1-A10, B1-B10	25
11	CSSZ 37-46	Central and South America	A37-A46, B37-B46	25
12	CSSZ 89-98	Central and South America	A89-A98, B89-B98	25
13	CSSZ 102 – 111	Central and South America	A102-A111, B102-B111	25
14	NTSZ 30-39	New Zealand-Kermadec-Tonga	A30-A39, B30-B39	25
15	NVSZ 28-37	New Britain-Solomons-Vanuatu	A28-A37, B28-B37	25
16	MOSZ 1-10	ManusOCB	A1-A10, B1-B10	25
17	NGSZ 3-12	North New Guinea	A3-A12, B3-B12	25
18	EPSZ 6-15	East Philippines	A6-A15, B6-B15	25
19	RNSZ 12-21	Ryukus-Kyushu-Nankai	A12-A21, B12-B21	25
		Mw 7.5 Tsunami scenario		
20	NTSZ B36	New Zealand-Kermadec-Tonga	B36	1

Micro-tsunami scenario

21	ACSZ B6	Aleutian-Alaska-Cascadia	B6	0.05

Table 3 Unit source combinations used to generate synthetic mega-tsunami scenarios for robustness and stability testing of the Chignik forecast model.

Figures

Figure 1 Image of Chignik and Anchorage Bay (courtesy of US Fish and Wildlife Service).

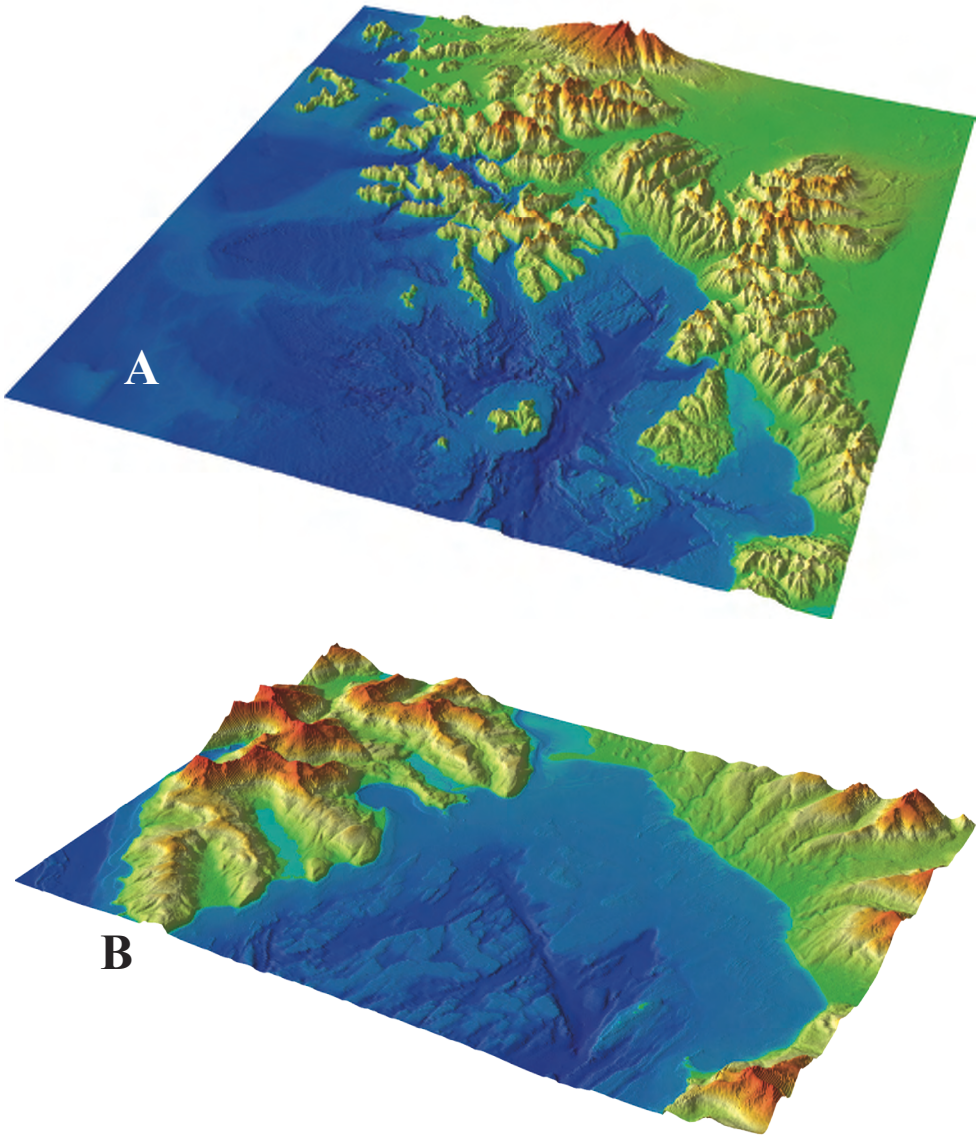

Figure 2 Perspective views of the Chignik DEMs. A)1 arc-second Chignik DEM from the northeast. B) 1/3 arc-second Chignik DEM from the northeast. (Courtesy of NGDC)

Figure 3 Satellite image of Anchorage Bay (Alaska Department of Community and Regional Affairs).

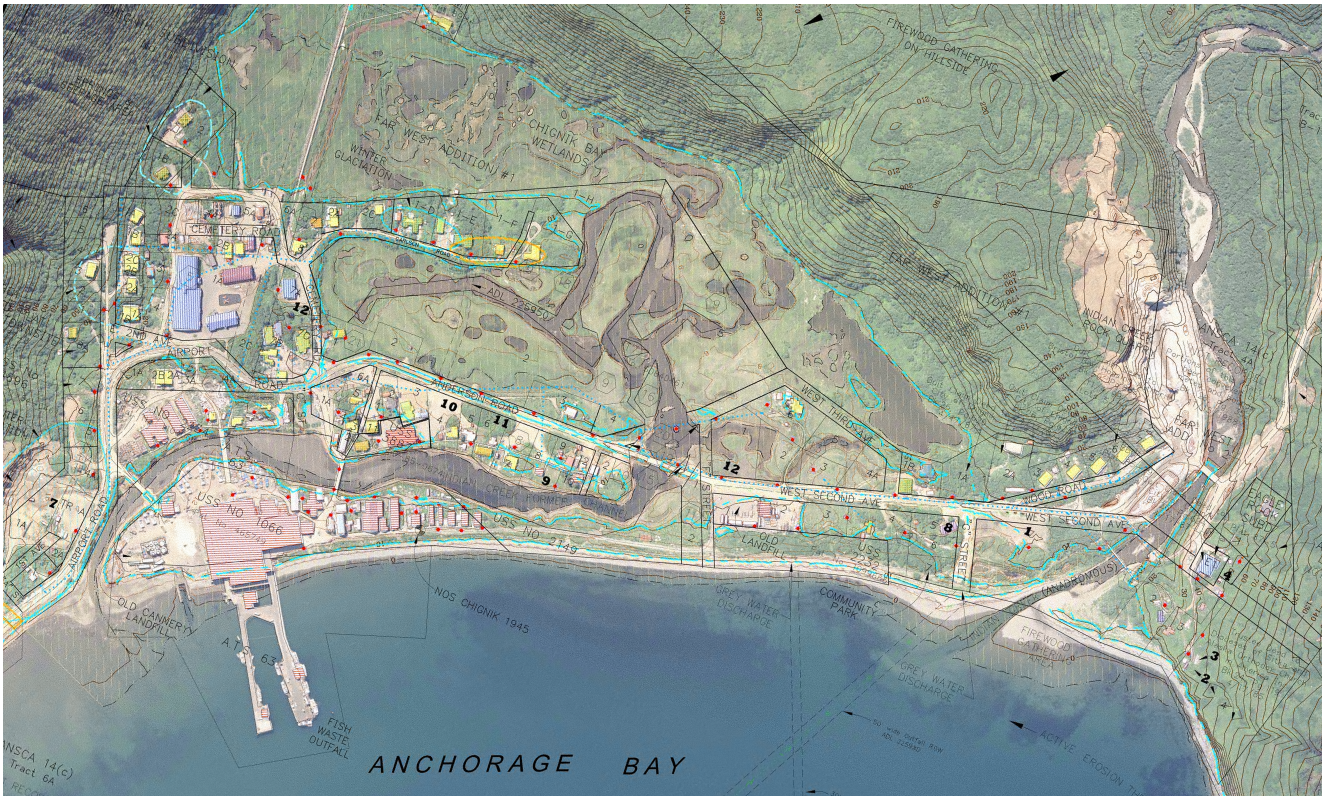

Figure 4 Satellite image of Chignik, with topography and community details overlaid (Alaska Department of Community and Regional Affairs).

Figure 5 Image of the beach profile in front of Chignik (Alaska Department of Community and Regional Affairs).

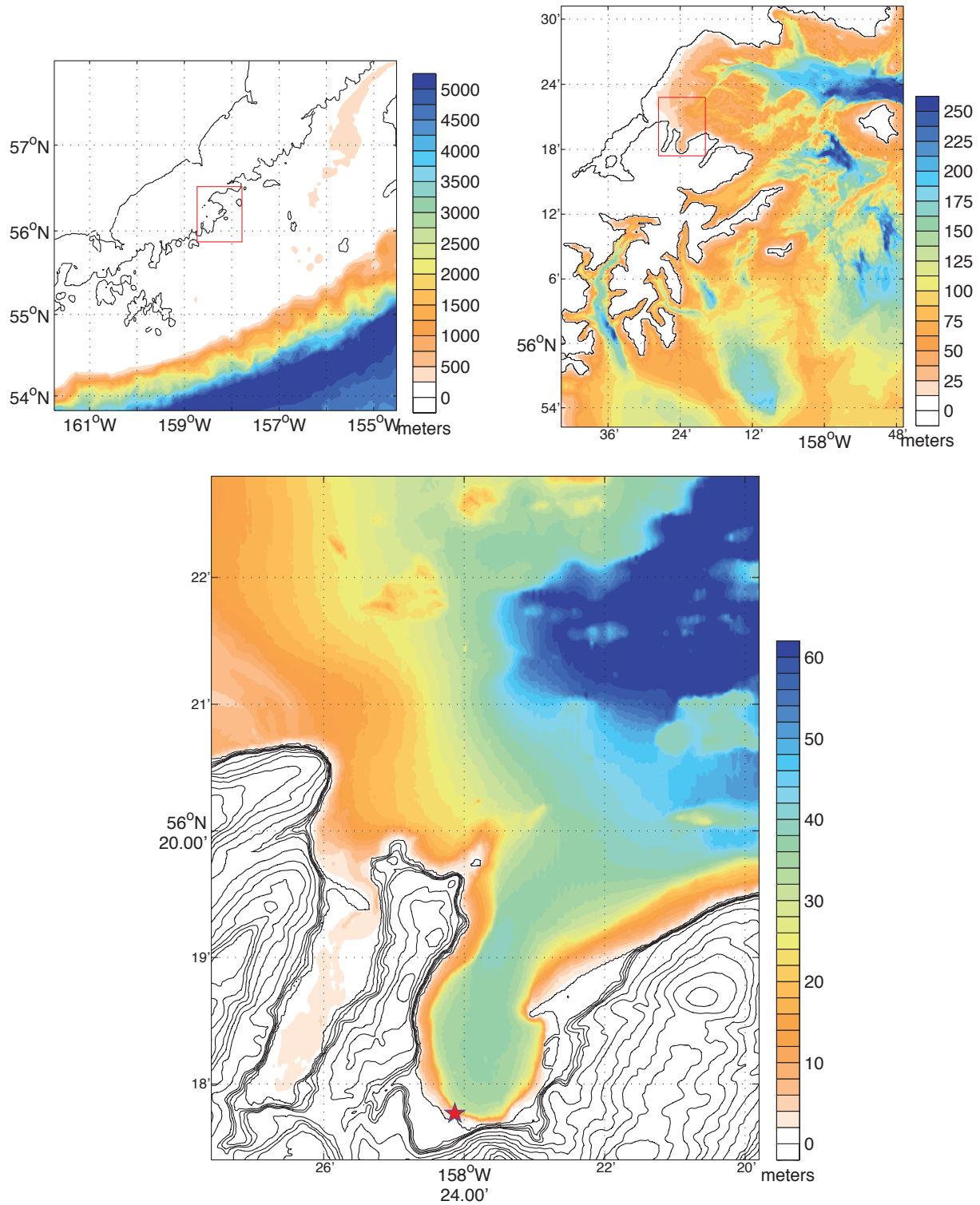

Figure 6 Bathymetry (meters) for the reference inundation model grids. The A grid is shown in the top left panel, the B grid in the bottom left panel, and the C grid in the right panel. The topography of the C grid is shown using contours with 10 meter intervals from 0 to 40 and then 40 meters intervals for higher values. The red boxes in the A and B plots show the position of the nested B and C grids, respectively. The red star shows the location of the Chignik warning point.

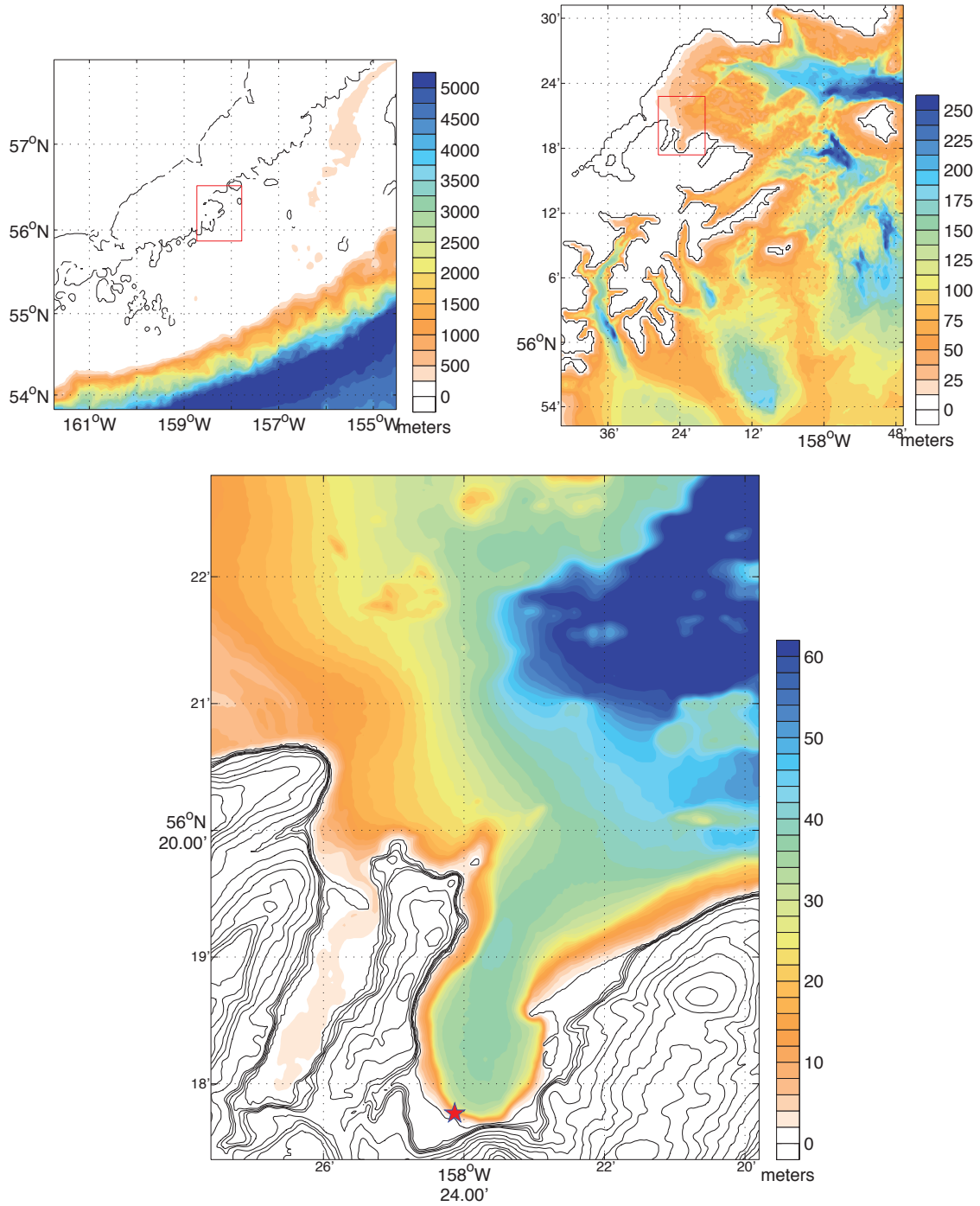

Figure 7 Bathymetry (meters) for the forecast inundation model grids. The A grid is shown in the top left panel, the B grid in the bottom left panel, and the C grid in the right panel. The topography of the C grid is shown using contours with 10 meter intervals from 0 to 40 and then 40 meters intervals for higher values. The red boxes in the A and B plots show the position of the nested B and C grids, respectively. The red star shows the location of the Chignik warning point.

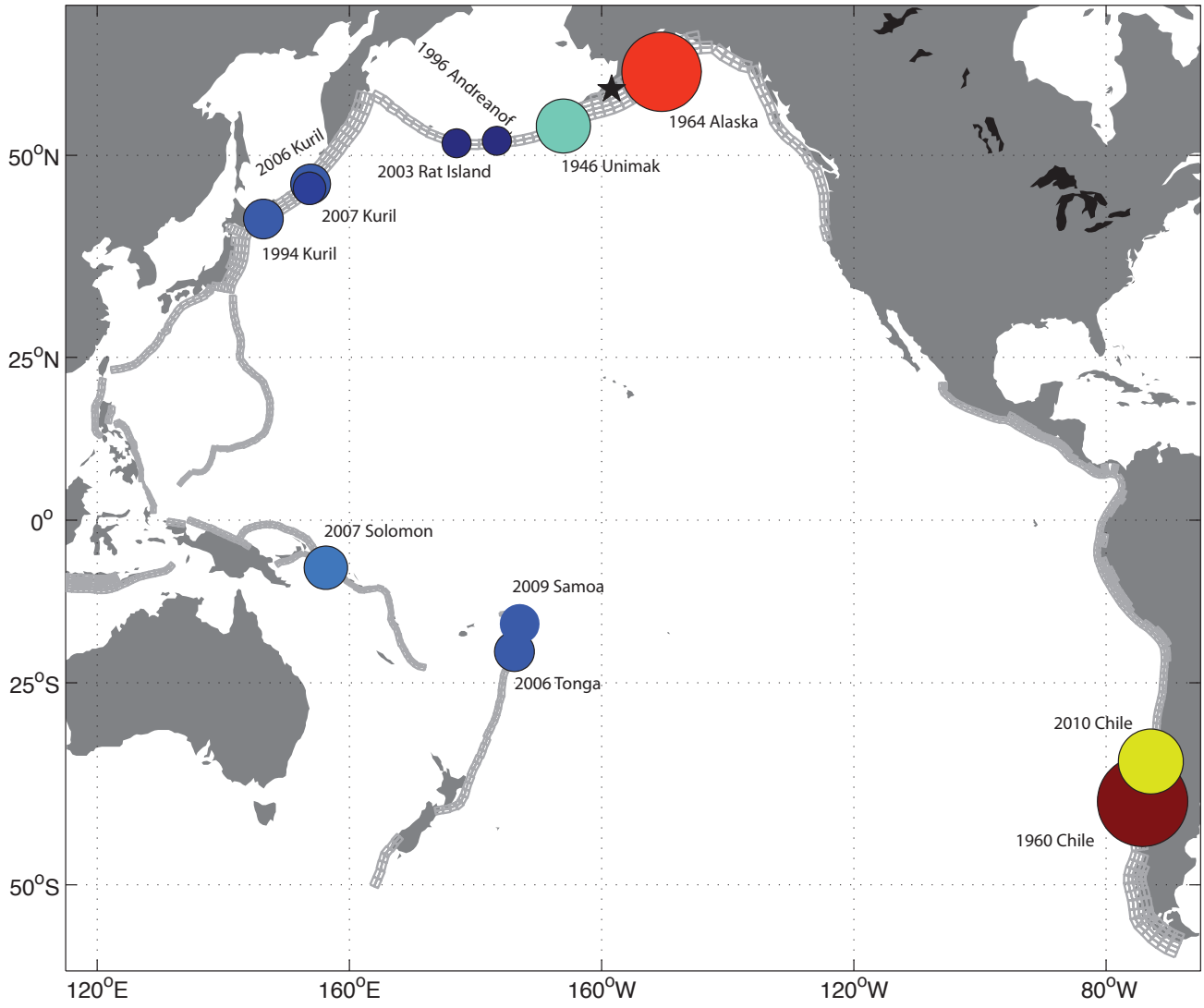

Figure 8 Map of the Pacific Ocean Basin showing the locations and magnitudes of the 12 historical events used to test and validate the Chignik model. Relative earthquake magnitude is shown by the varying sizes and colors of the filled circles. The largest magnitude earthquake used in model validation was the 196o Chile Mw 9.5 earthquake. The star denotes Chigniks's location.

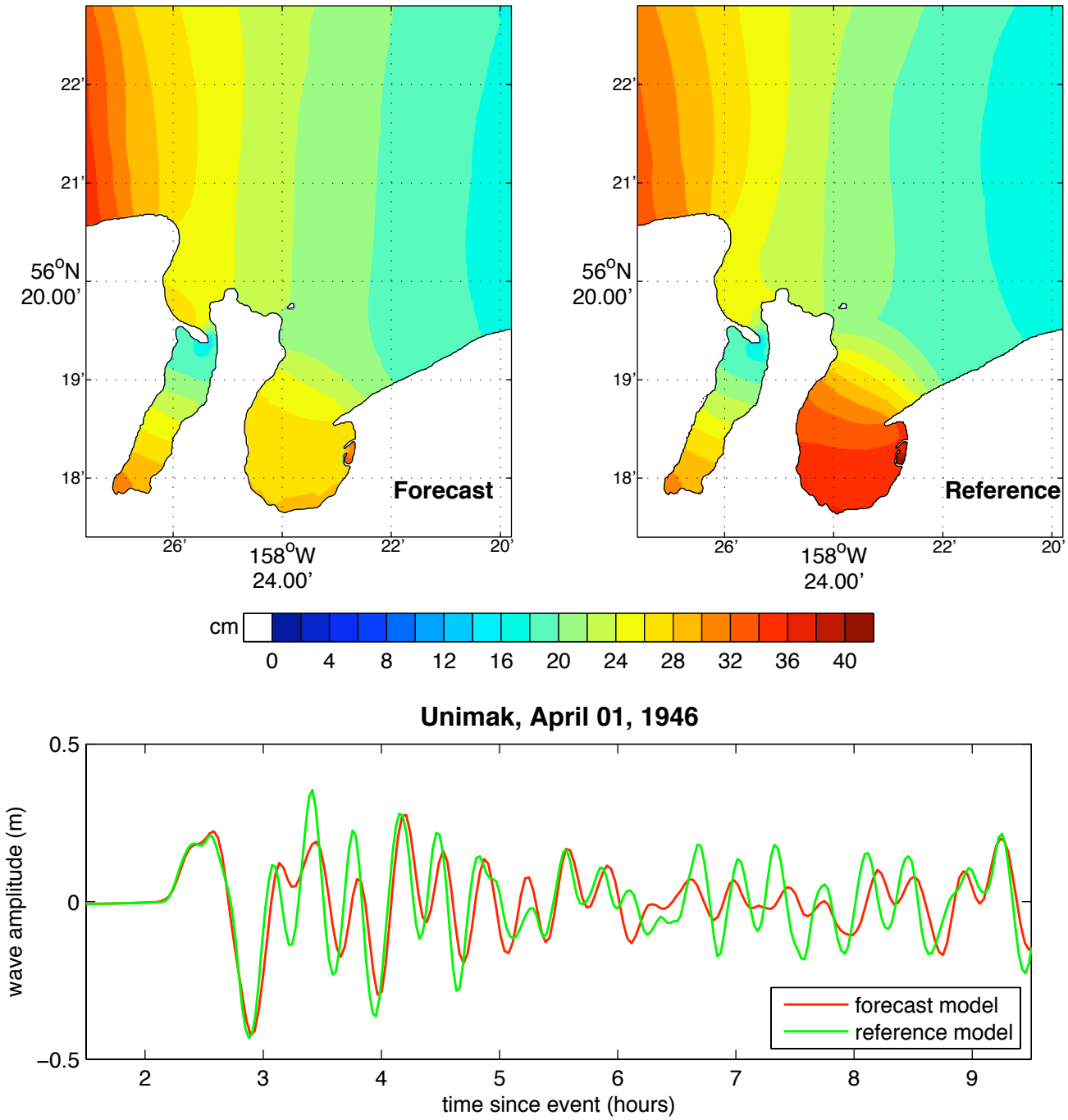

Figure 9 Model results for the 1946 Unimak Mw 8.5 event. The upper two panels show, respectively, the forecast and reference model maximum wave height predictions. The lower panel shows the forecast model (red) and reference model (green) wave amplitudes at the Chignik warning point location.

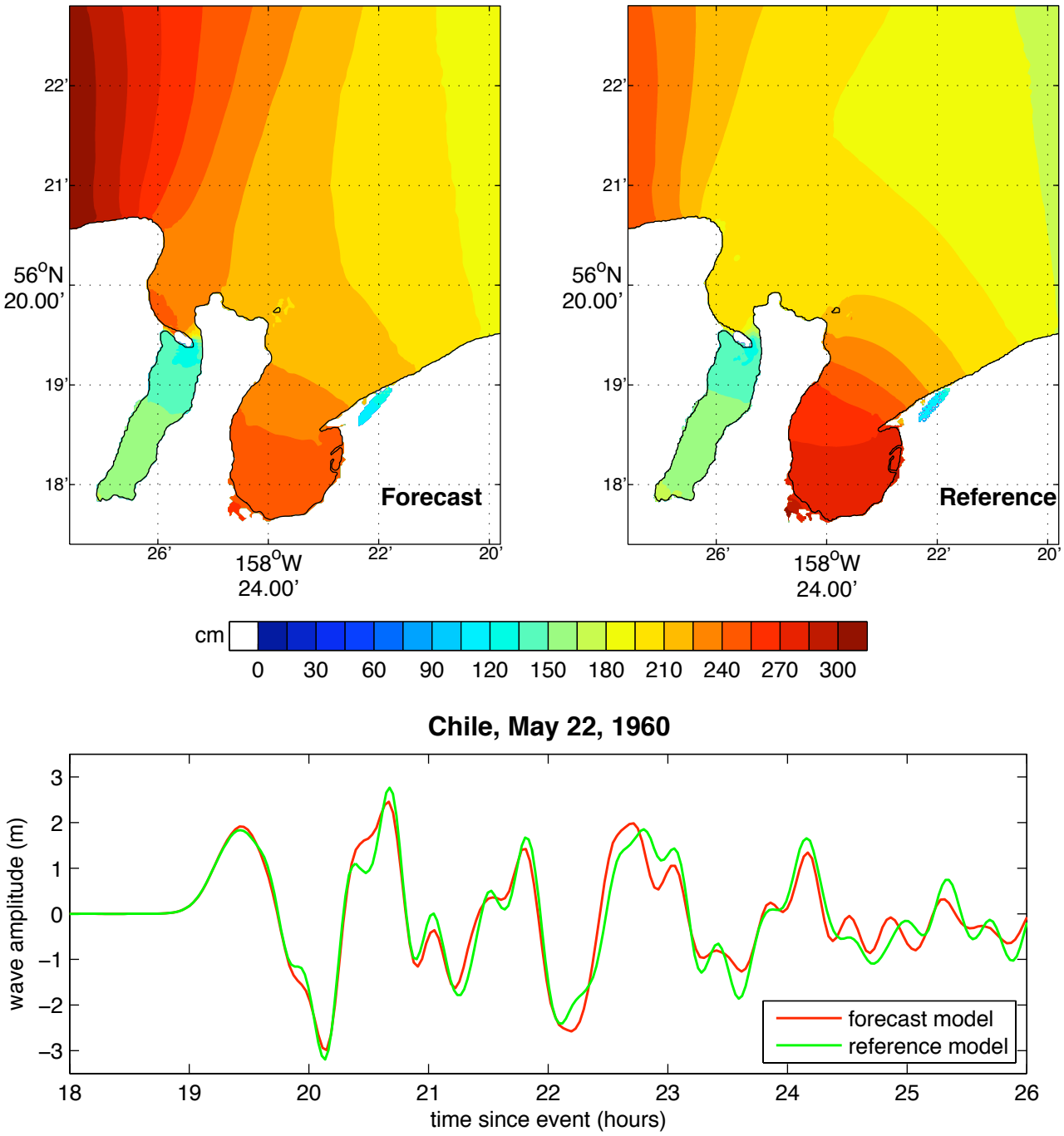

Figure 10 Model results results for the 1960 Chile Mw 9.5 event. The upper two panels show, respectively, the forecast and reference model maximum wave height predictions. The lower panel shows the forecast model (red) and reference model (green) wave amplitudes at the Chignik warning point location

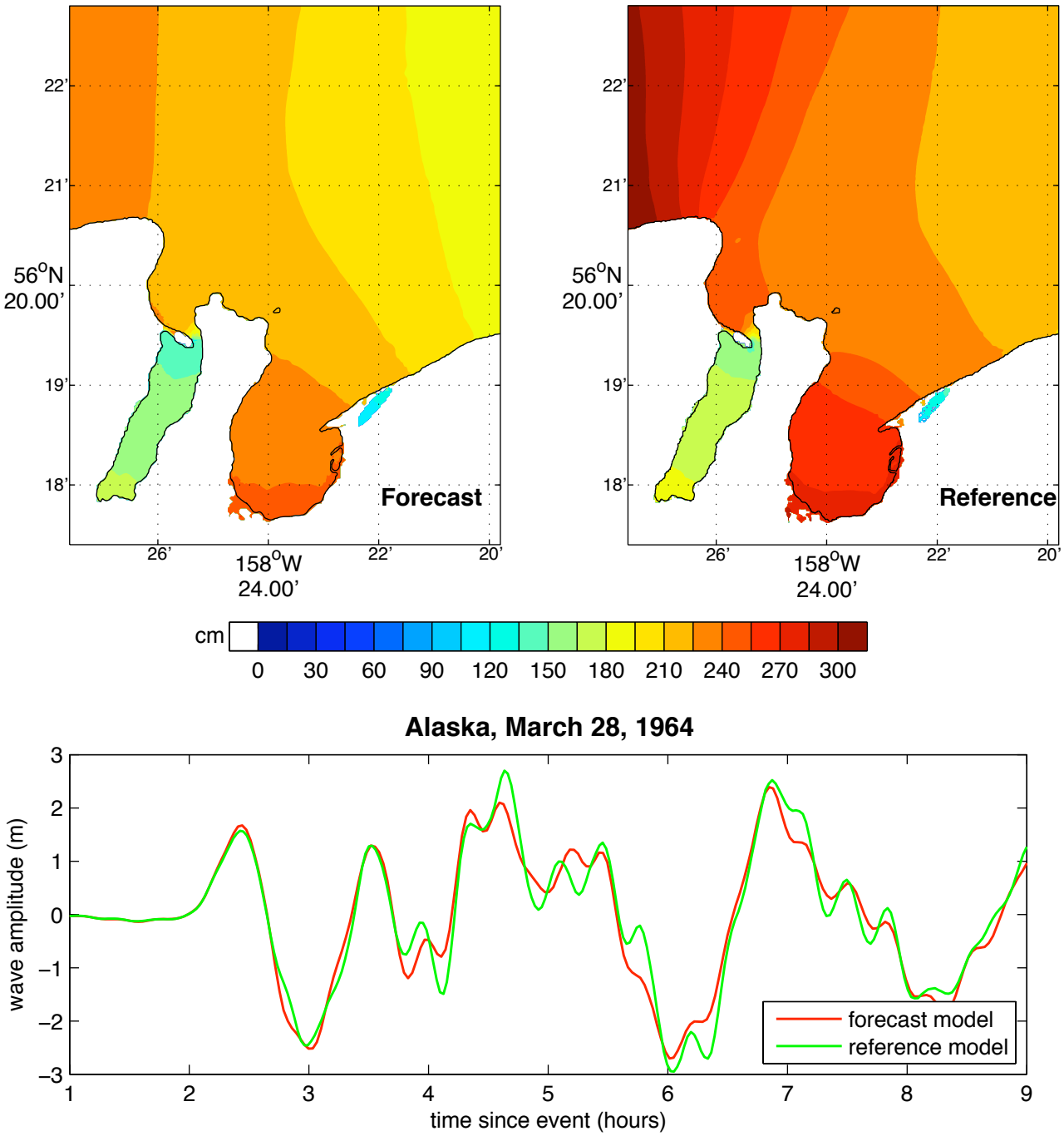

Figure 11 Model results for the 1964 Alaska Mw 9.2 event. The upper two panels show, respectively, the forecast and reference model maximum wave height predictions. The lower panel shows the forecast model (red) and reference model (green) wave amplitudes at the Chignik warning point location

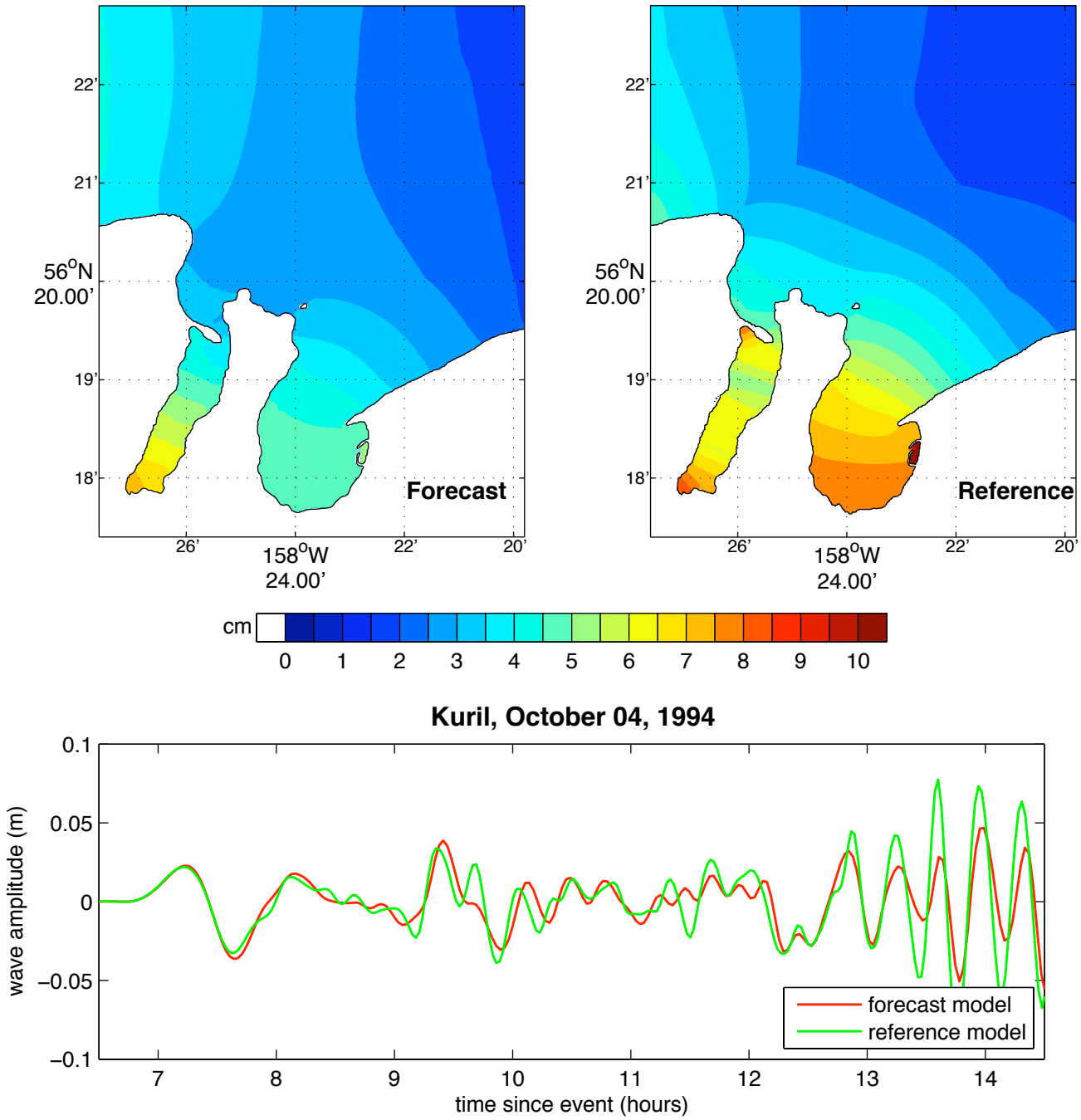

Figure 12 Model results for the 1994 Kuril Mw 8.3 event. The upper two panels show, respectively, the forecast and reference model maximum wave height predictions. The lower panel shows the forecast model (red) and reference model (green) wave amplitudes at the Chignik warning point location.

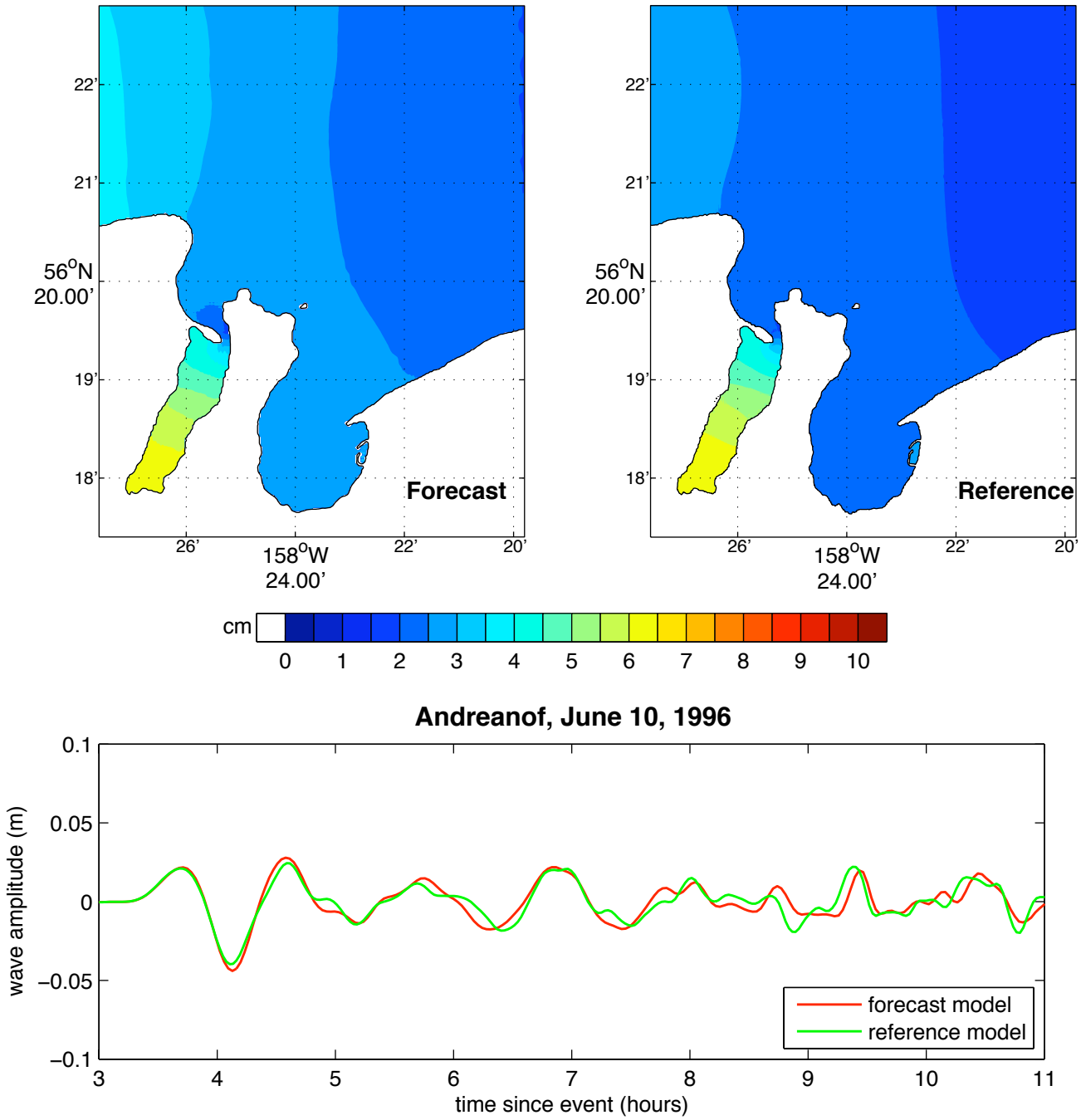

Figure 13 Model results for the 1996 Andreanof Mw 7.9 event. The upper two panels show, respectively, the forecast and reference model maximum wave height predictions. The lower panel shows the forecast model (red) and reference model (green) wave amplitudes at the Chignik warning point location.

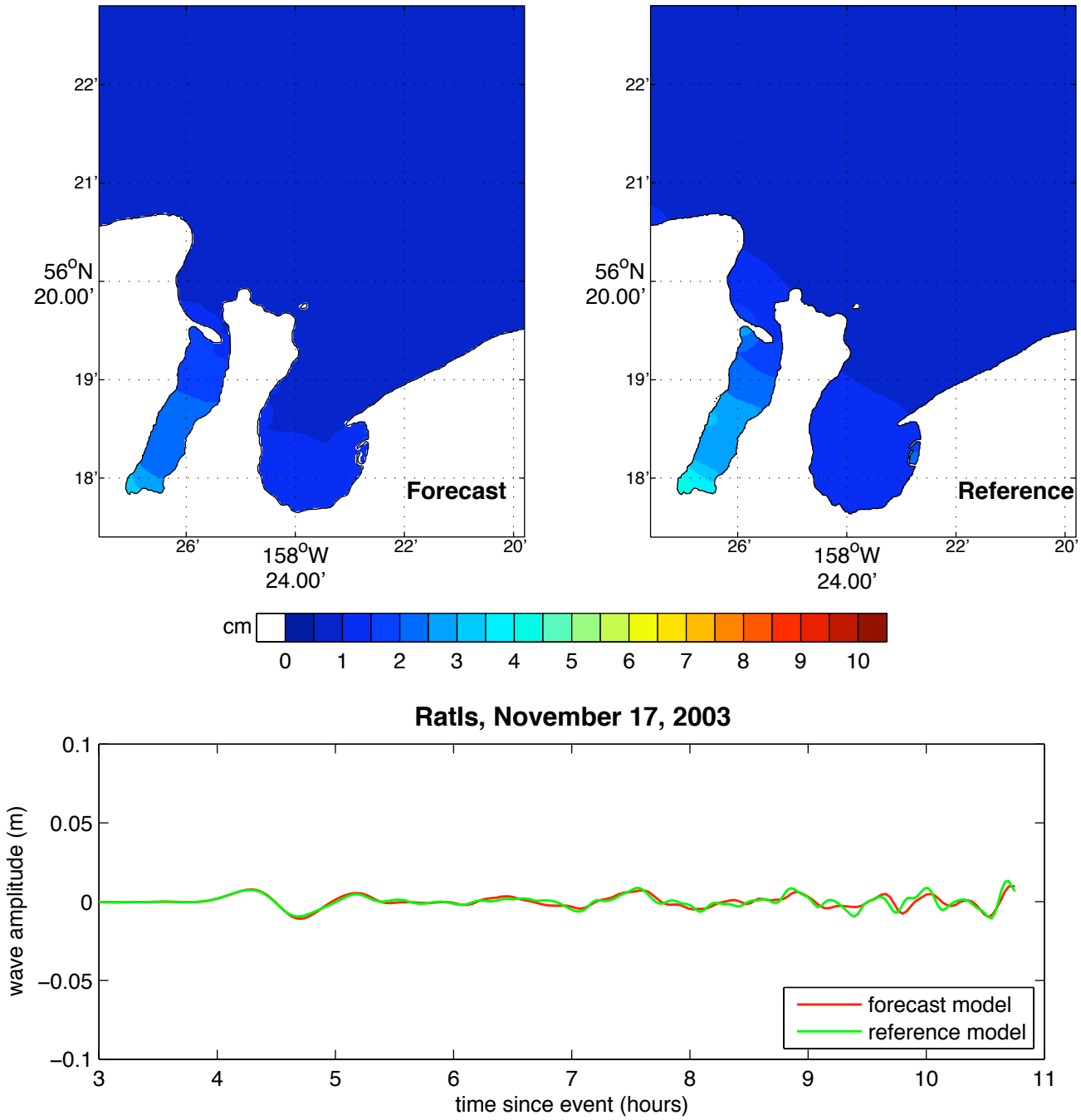

Figure 14 Model results for the 2003 Rat Island Mw 7.7 event. The upper two panels show, respectively, the forecast and reference model maximum wave height predictions. The lower panel shows the forecast model (red) and reference model (green) wave amplitudes at the Chignik warning point location.

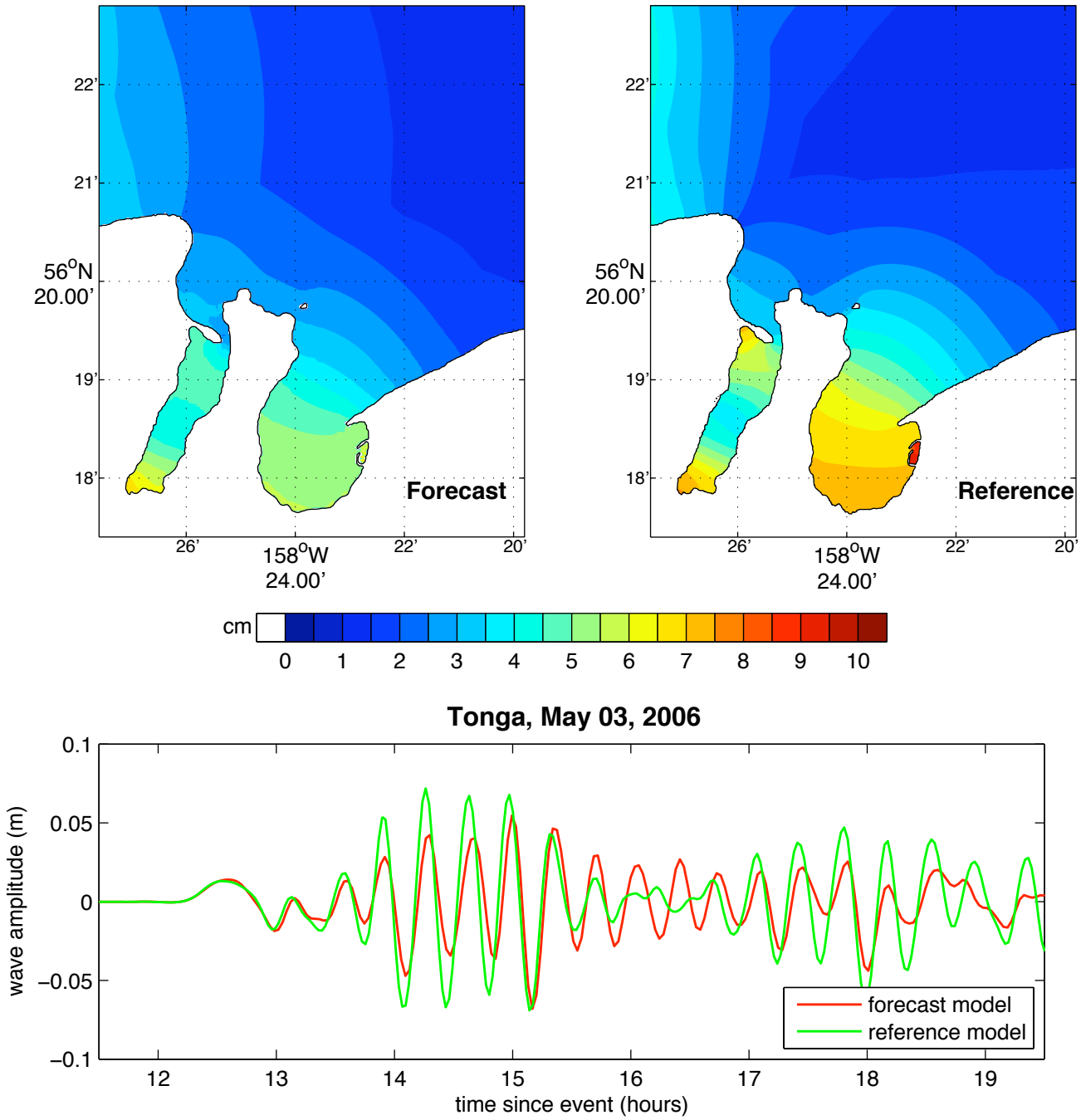

Figure 15 Model results for the 2006 Tonga Mw 8.0 event. The upper two panels show, respectively, the forecast and reference model maximum wave height predictions. The lower panel shows the forecast model (red) and reference model (green) wave amplitudes at the Chignik warning point location.

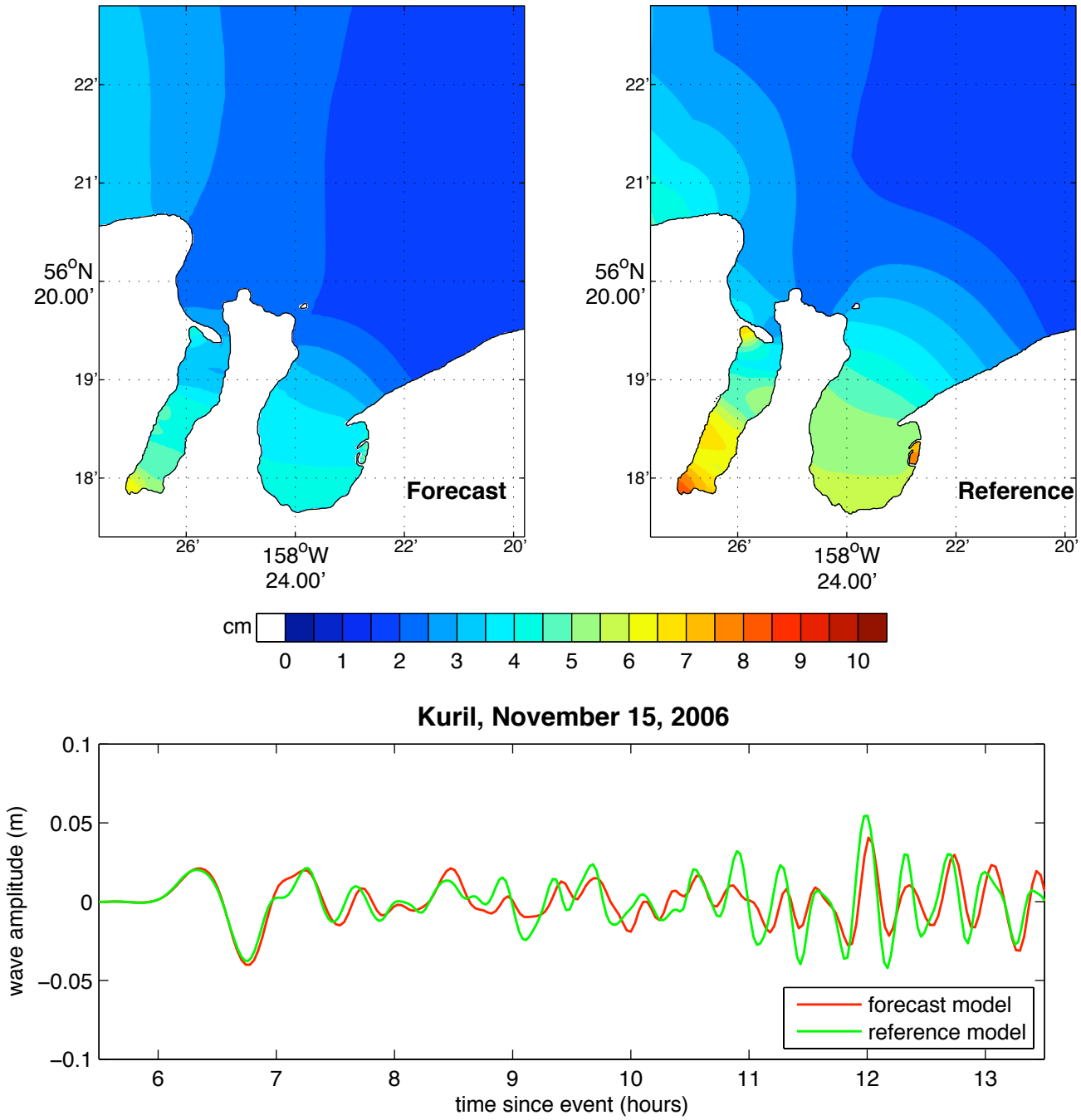

Figure 16 Model results for the 2006 Kuril Mw 8.3 event. The upper two panels show, respectively, the forecast and reference model maximum wave height predictions. The lower panel shows the forecast model (red) and reference model (green) wave amplitudes at the Chignik warning point location.

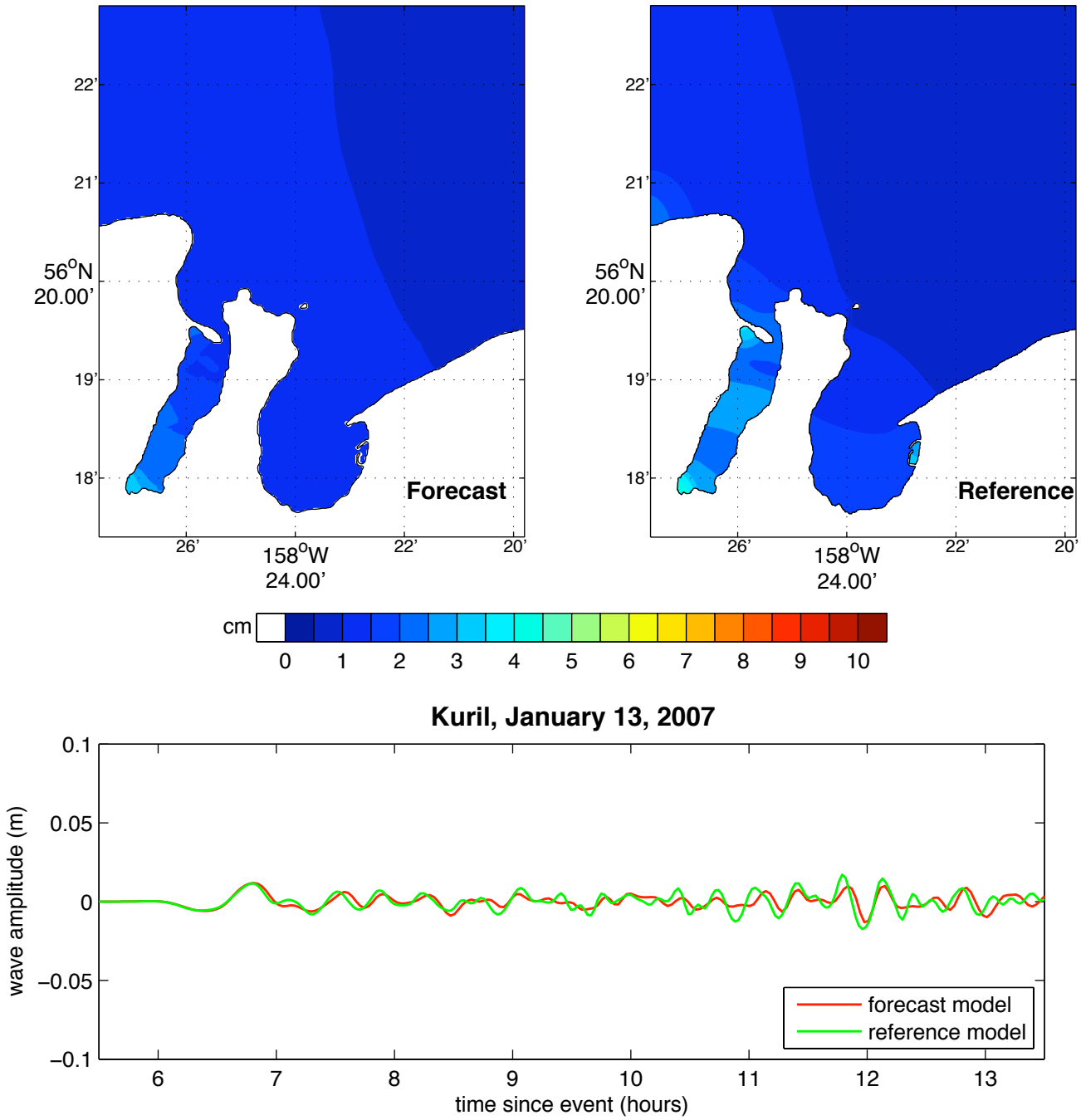

Figure 17 Model results for the 2007 Kuril Mw 8.1 event. The upper two panels show, respectively, the forecast and reference model maximum wave height predictions. The lower panel shows the forecast model (red) and reference model (green) wave amplitudes at the Chignik warning point location.

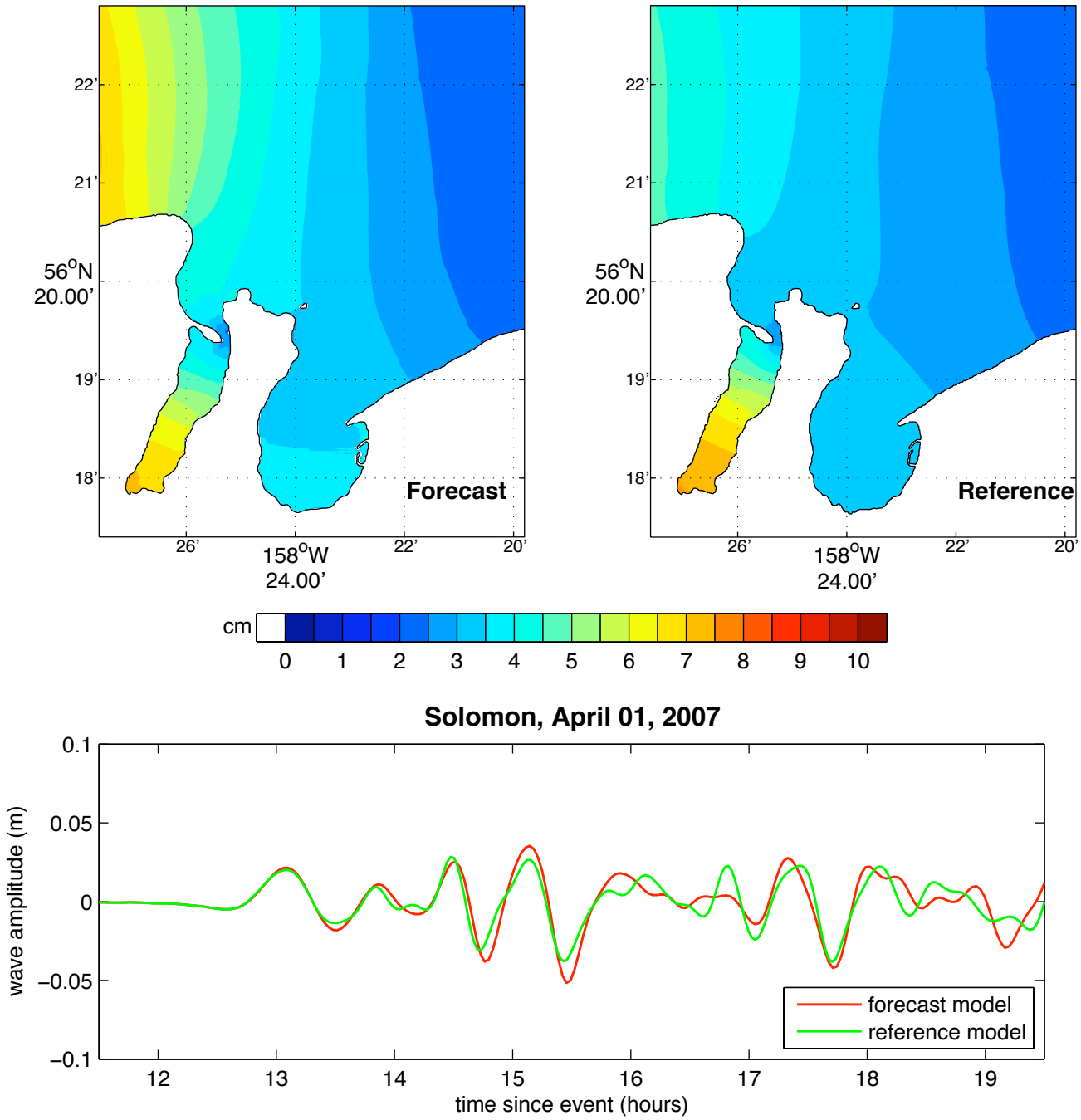

Figure 18 Model results for the 2007 Solomon Mw 8.1 event. The upper two panels show, respectively, the forecast and reference model maximum wave height predictions. The lower panel shows the forecast model (red) and reference model (green) wave amplitudes at the Chignik warning point location.

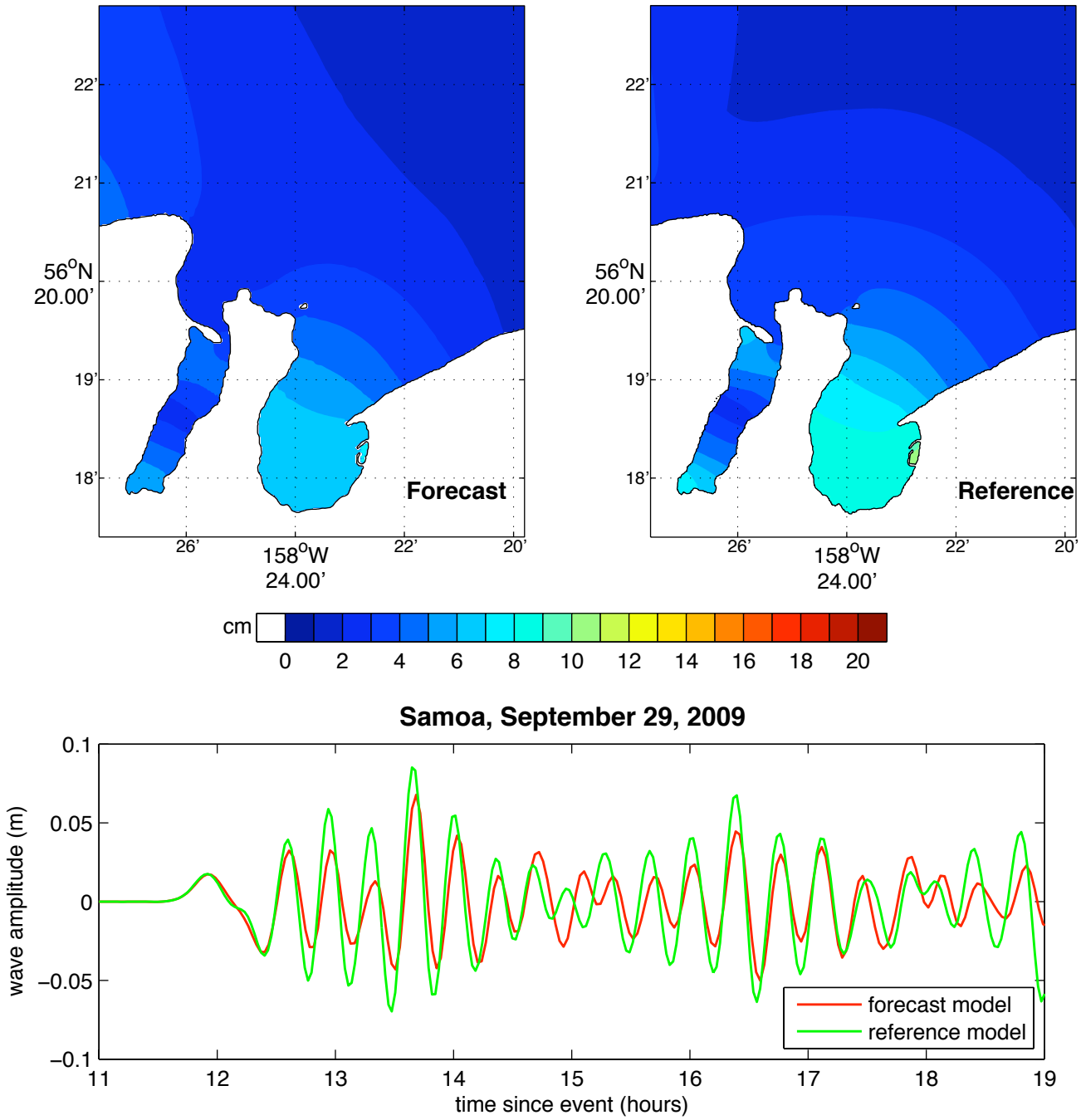

Figure 19 Model results for the 2009 Samoa Mw 8.0 event. The upper two panels show, respectively, the forecast and reference model maximum wave height predictions. The lower panel shows the forecast model (red) and reference model (green) wave amplitudes at the Chignik warning point location.

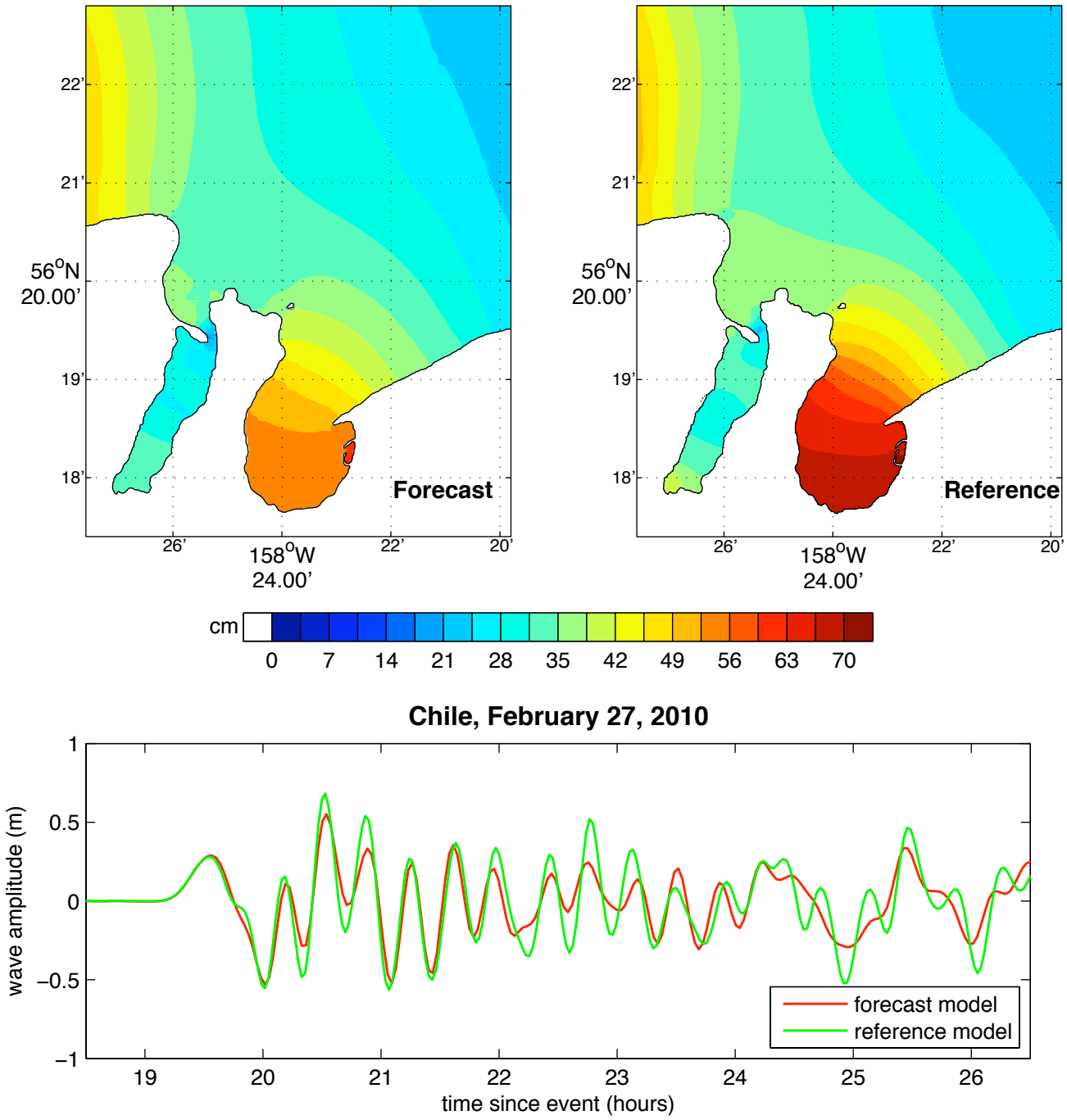

Figure 20 Model results for the 2010 Chile Mw 8.8 event. The upper two panels show, respectively, the forecast and reference model maximum wave height predictions. The lower panel shows the forecast model (red), reference model (green) and observed (black) wave amplitudes at the Chignik warning point location.

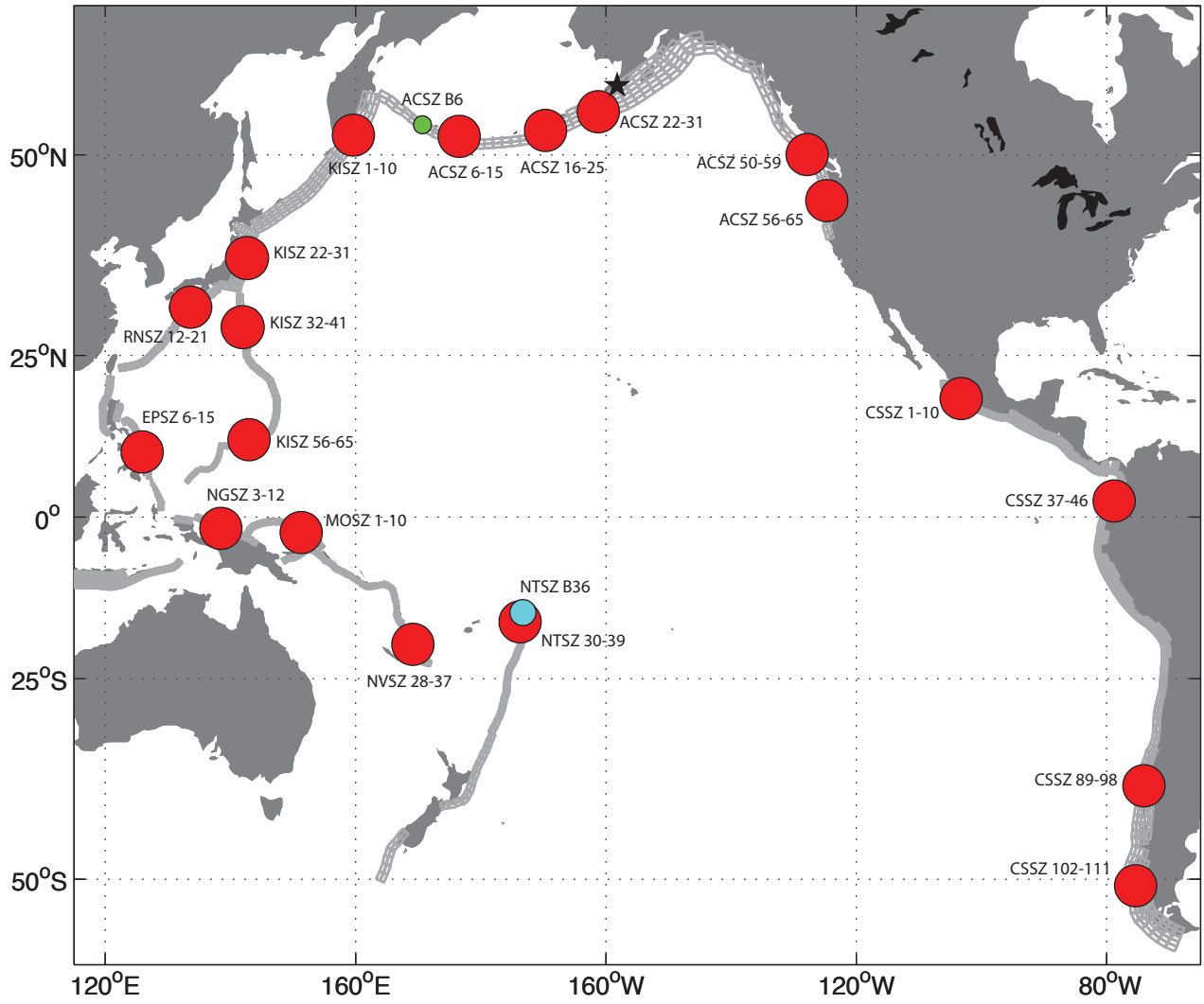

Figure 21 Map of the Pacific Ocean Basin showing the locations of the 19 simulated Mw 9.3 events (red circles) and the medium and micro events used to test and validate the Chignik model. The solid star denotes the location of Chignik.

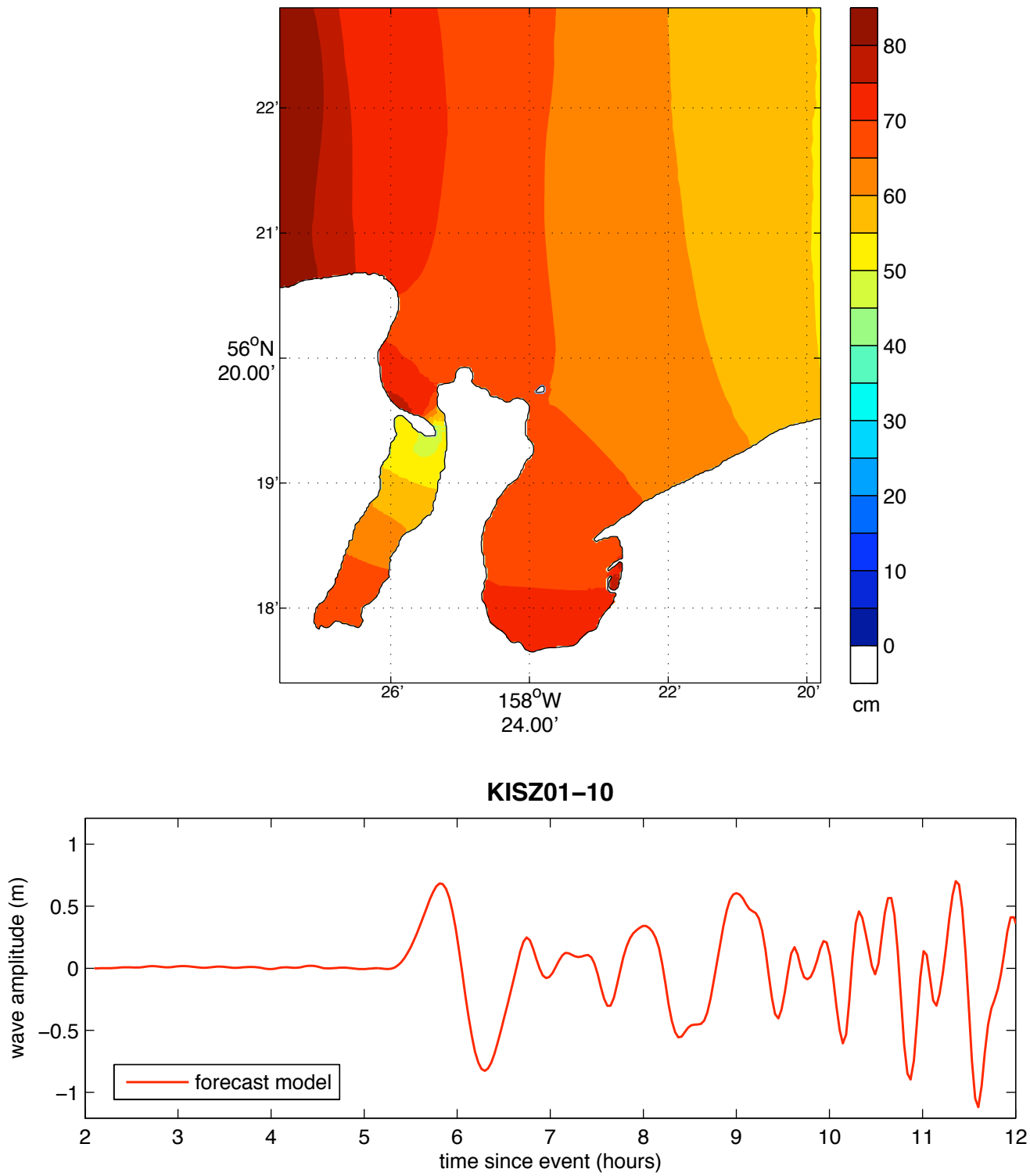

Figure 22 Results from the forecast model for the KISZ 1-10 synthetic event. The upper panel shows the map of predicted maximum wave height in the Chignik C-grid and the lower panel shows the time series of wave amplitude at the warning point location.

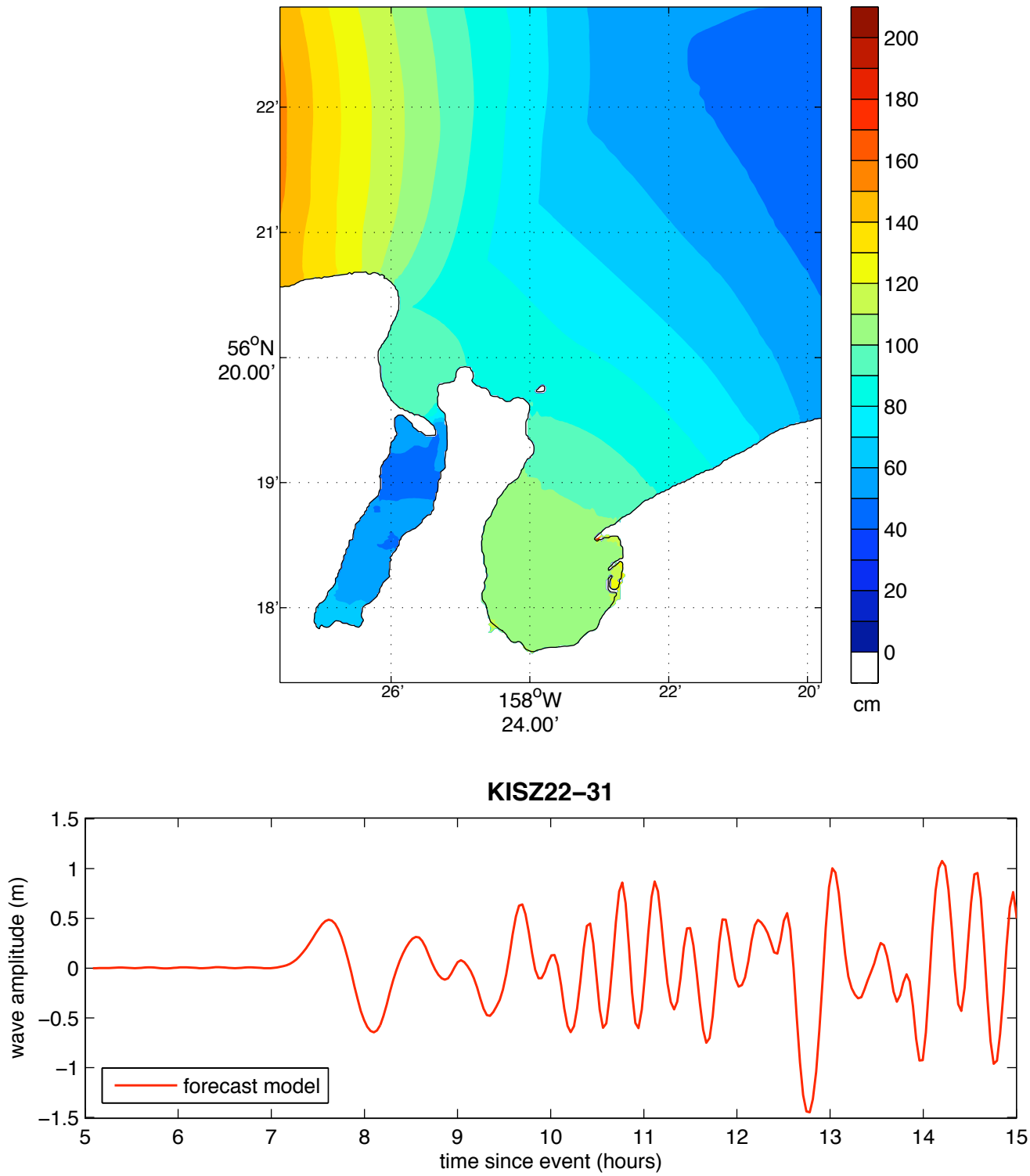

Figure 23 Results from the forecast model for the KISZ 22-31 synthetic event. The upper panel shows the map of predicted maximum wave height in the Chignik C-grid and the lower panel shows the time series of wave amplitude at the warning point location.

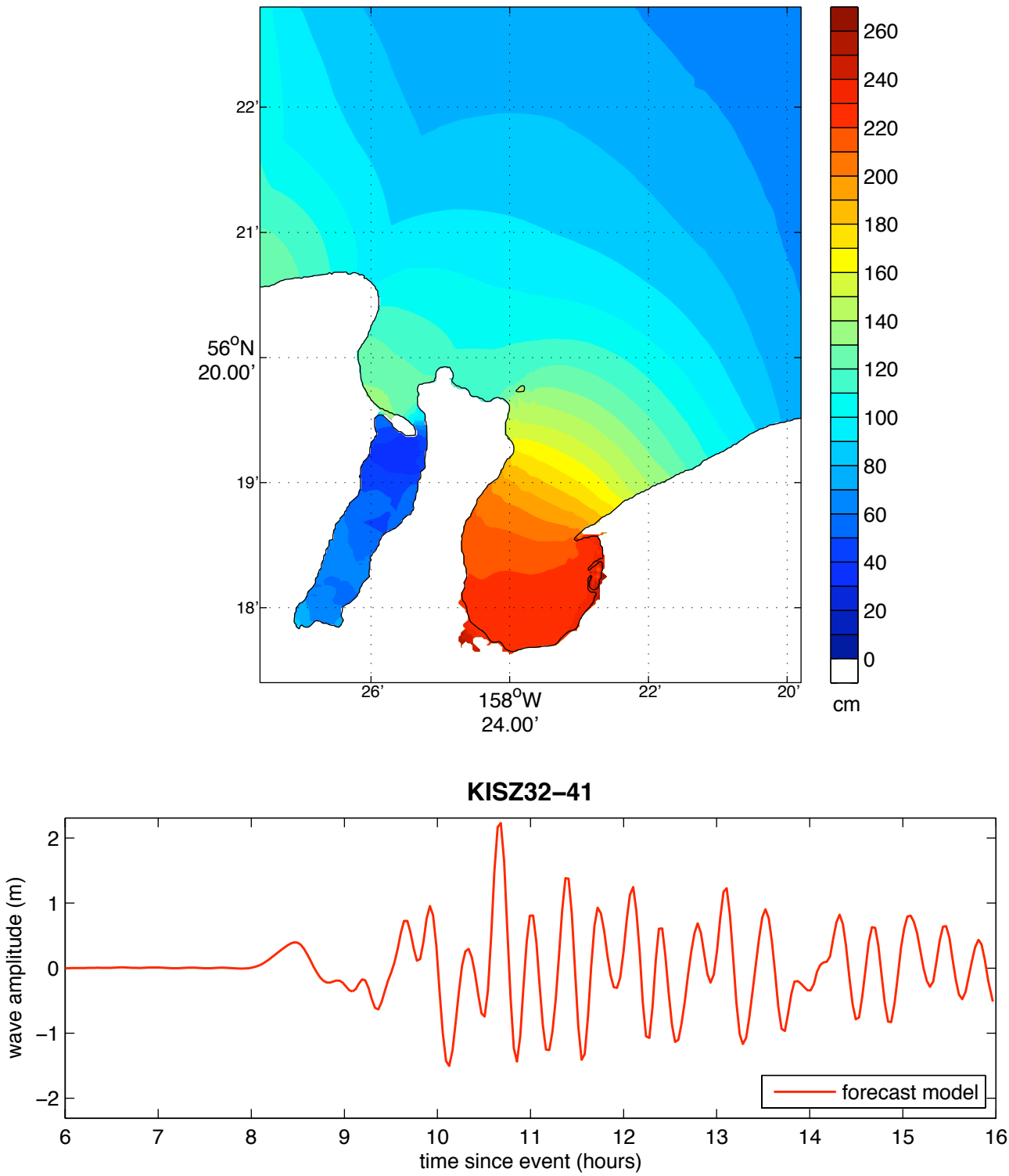

Figure 24 Results from the forecast model for the KISZ 32-41 synthetic event. The upper panel shows the map of predicted maximum wave height in the Chignik C-grid and the lower panel shows the time series of wave amplitude at the warning point location.

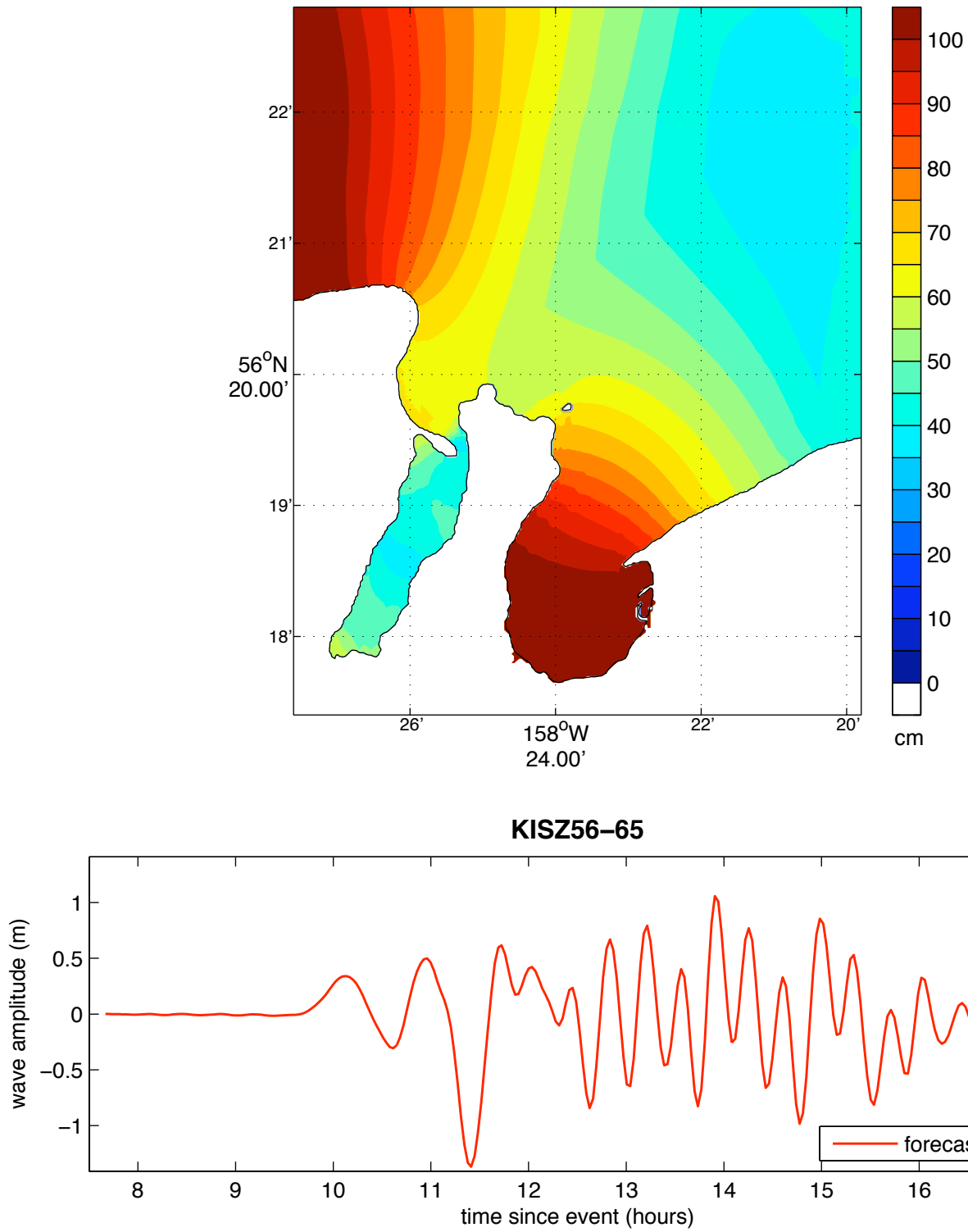

Figure 25 Results from the forecast model for the KISZ 56-65 synthetic event. The upper panel shows the map of predicted maximum wave height in the Chignik C-grid and the lower panel shows the time series of wave amplitude at the warning point location.

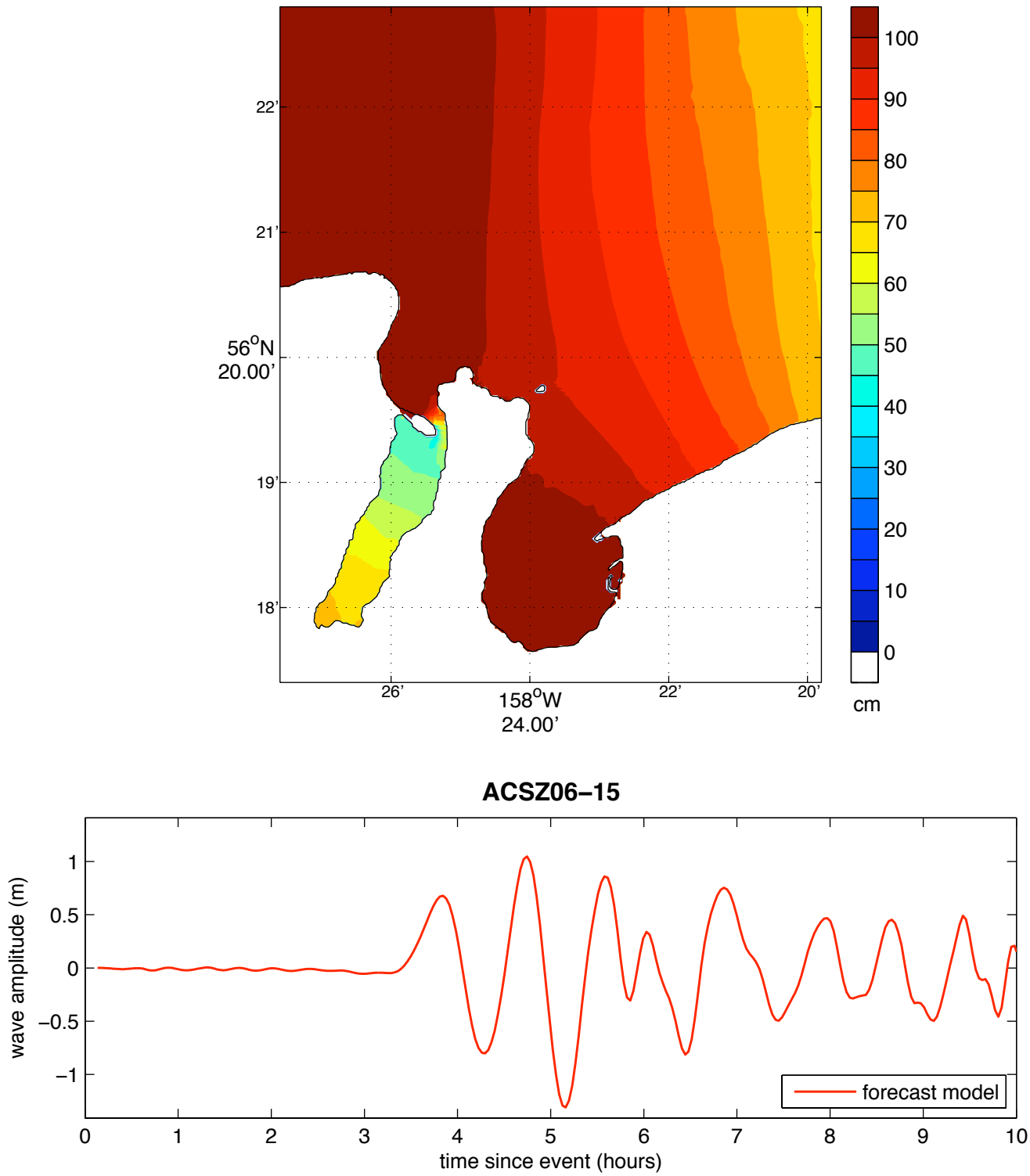

Figure 26 Results from the forecast model for the ACSZ 6-15 synthetic event. The upper panel shows the map of predicted maximum wave height in the Chignik C-grid and the lower panel shows the time series of wave amplitude at the warning point location.

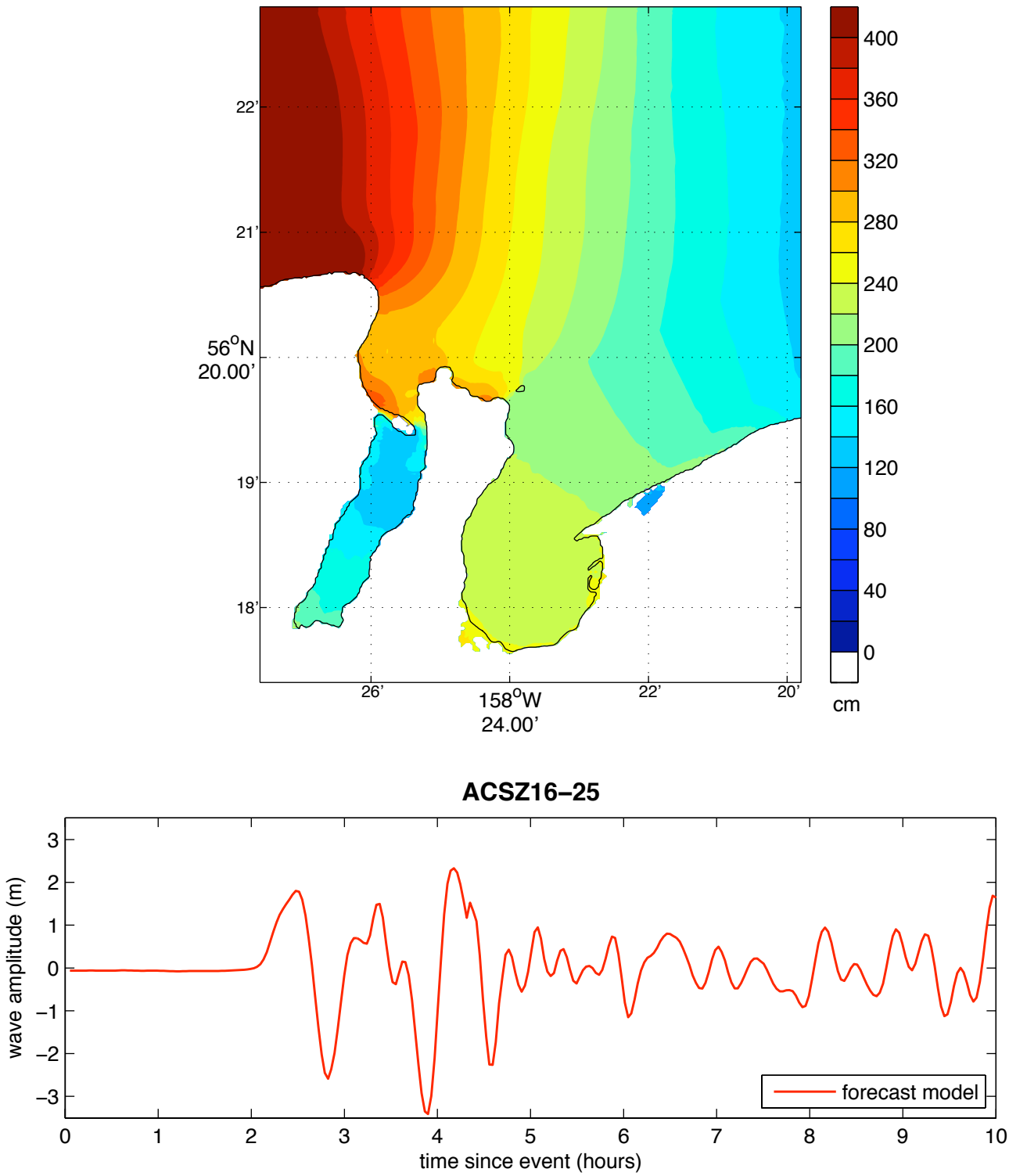

Figure 27 Results from the forecast model for the ACSZ 16-25 synthetic event. The upper panel shows the map of predicted maximum wave height in the Chignik C-grid and the lower panel shows the time series of wave amplitude at the warning point location.

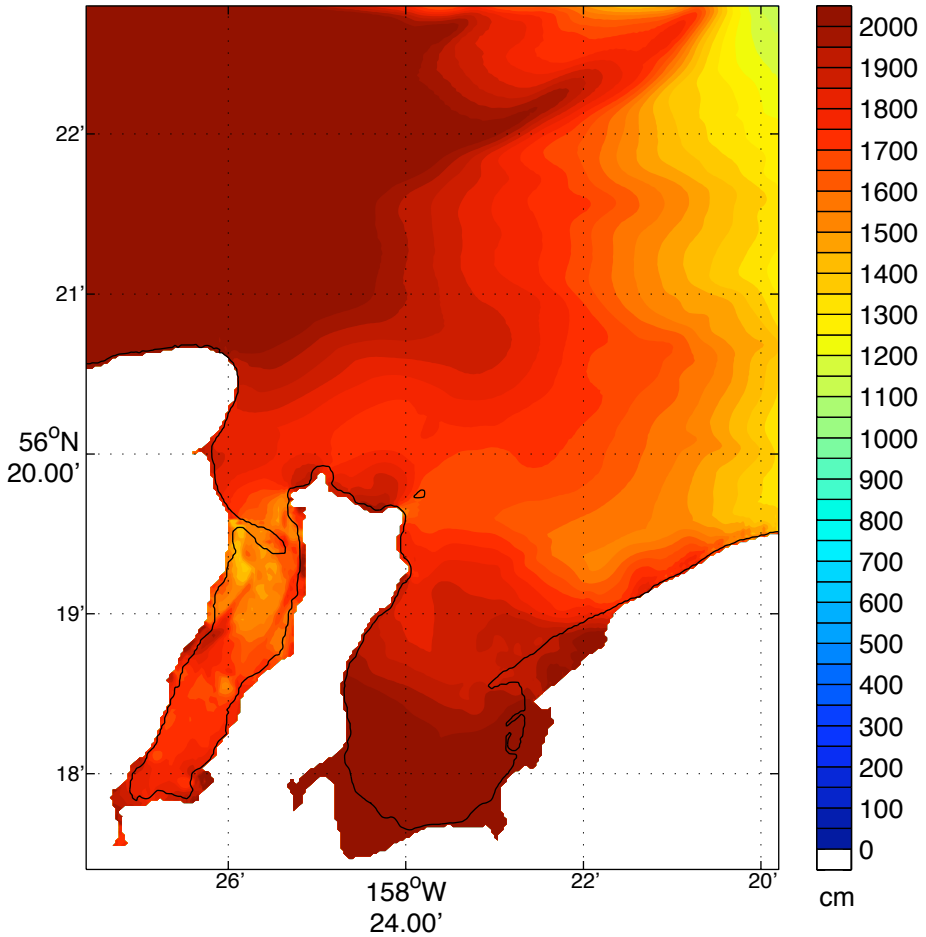

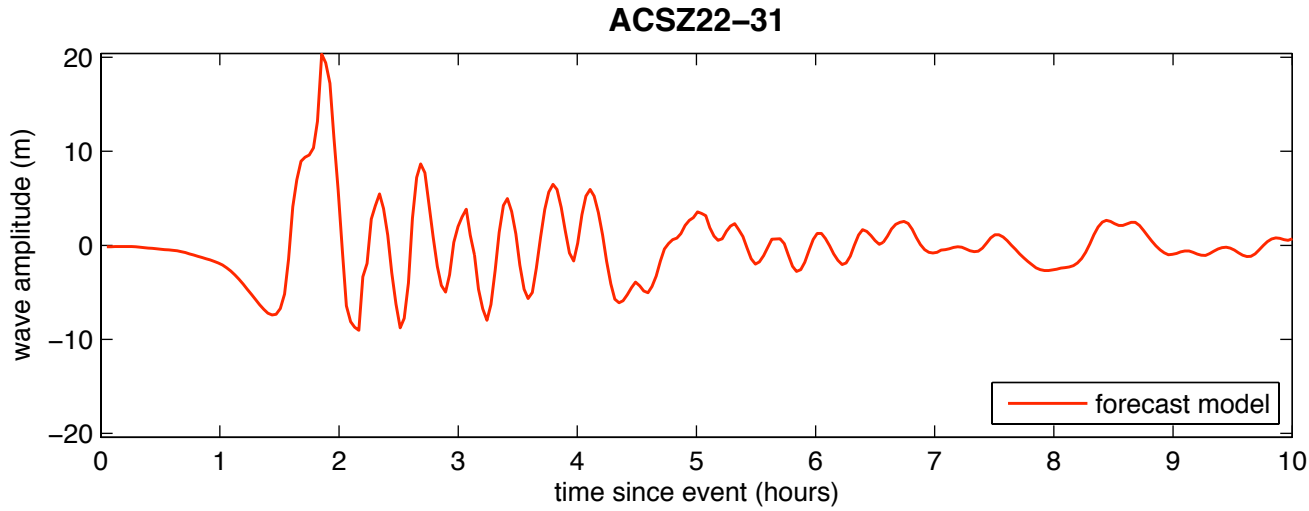

Figure 28 Results from the forecast model for the ACSZ 22-31 synthetic event. The upper panel shows the map of predicted maximum wave height in the Chignik C-grid and the lower panel shows the time series of wave amplitude at the warning point location.

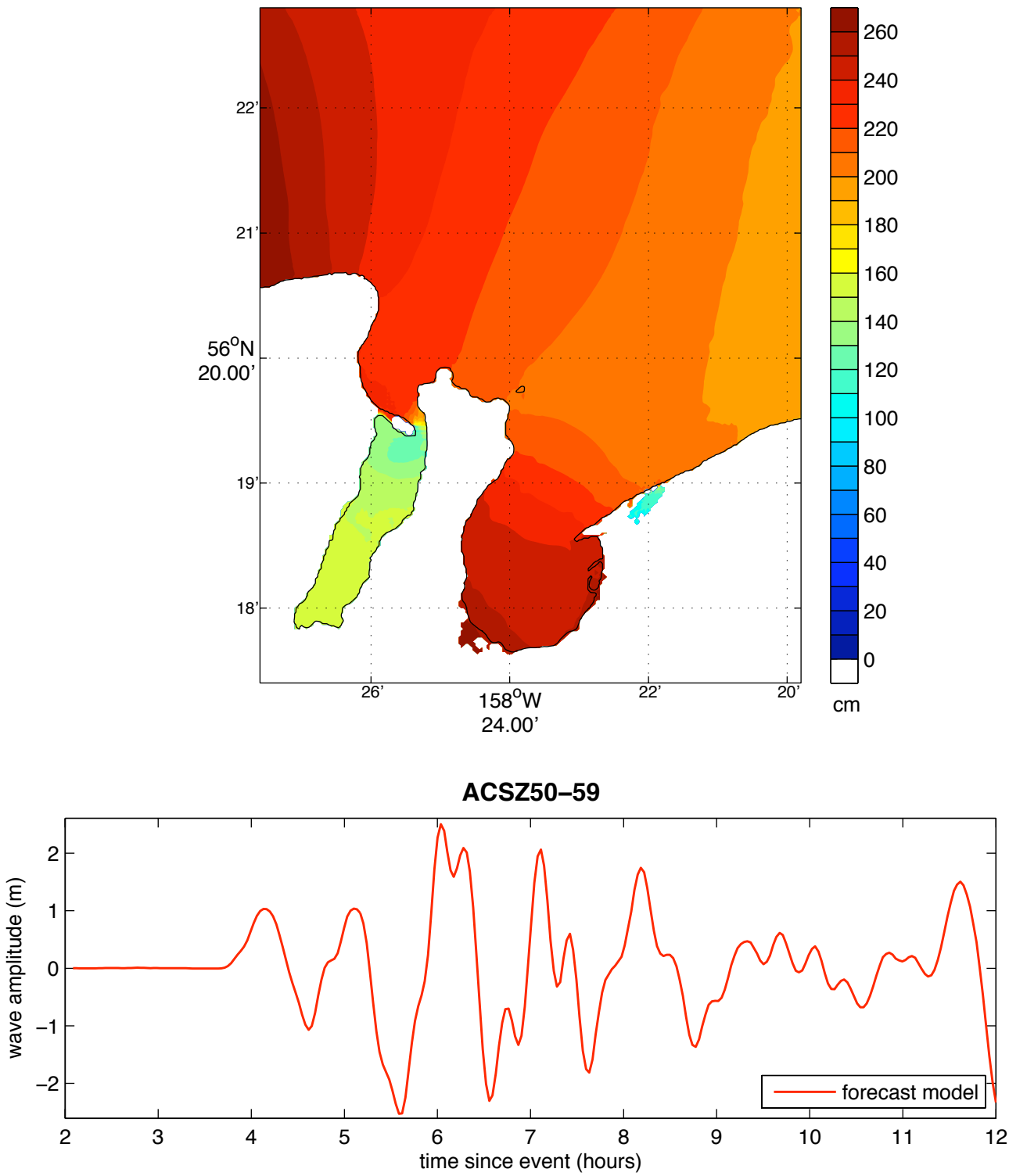

Figure 29 Results from the forecast model for the ACSZ 50-59 synthetic event. The upper panel shows the map of predicted maximum wave height in the Chignik C-grid and the lower panel shows the time series of wave amplitude at the warning point location.

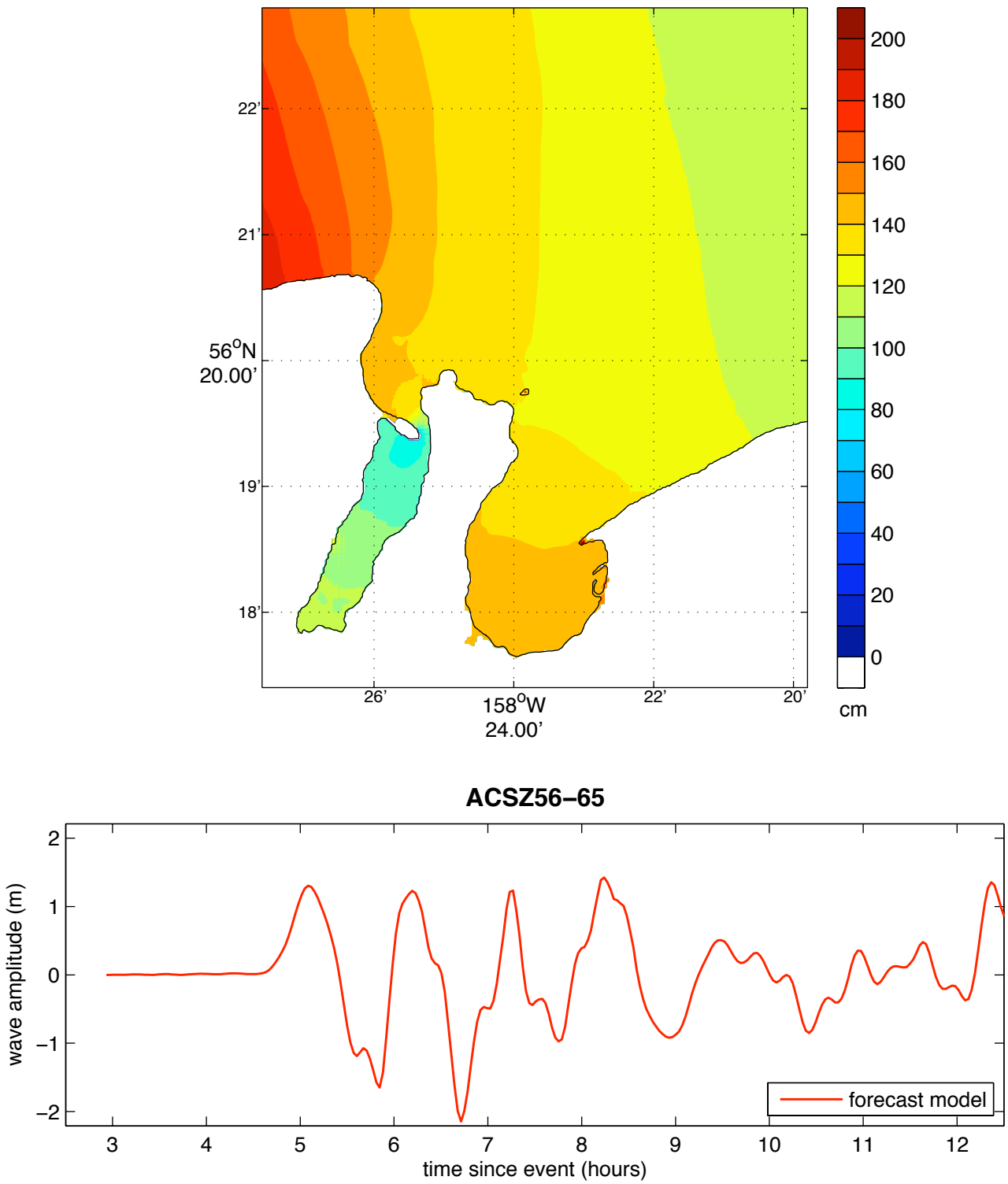

Figure 30 Results from the forecast model for the ACSZ 56-65 synthetic event. The upper panel shows the map of predicted maximum wave height in the Chignik C-grid and the lower panel shows the time series of wave amplitude at the warning point location.

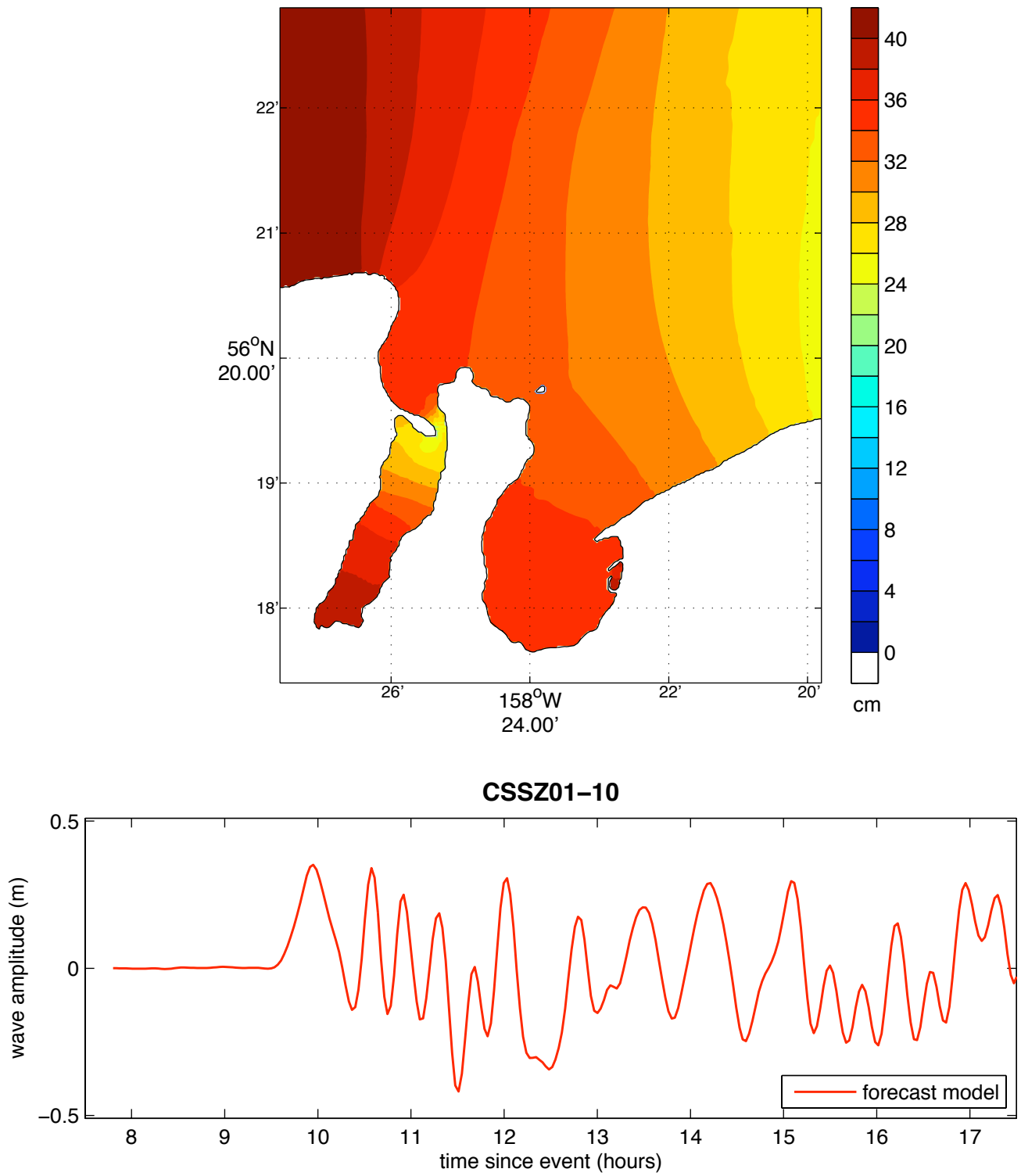

Figure 31 Results from the forecast model for the CSSZ 1-10 synthetic event. The upper panel shows the map of predicted maximum wave height in the Chignik C-grid and the lower panel shows the time series of wave amplitude at the warning point location.

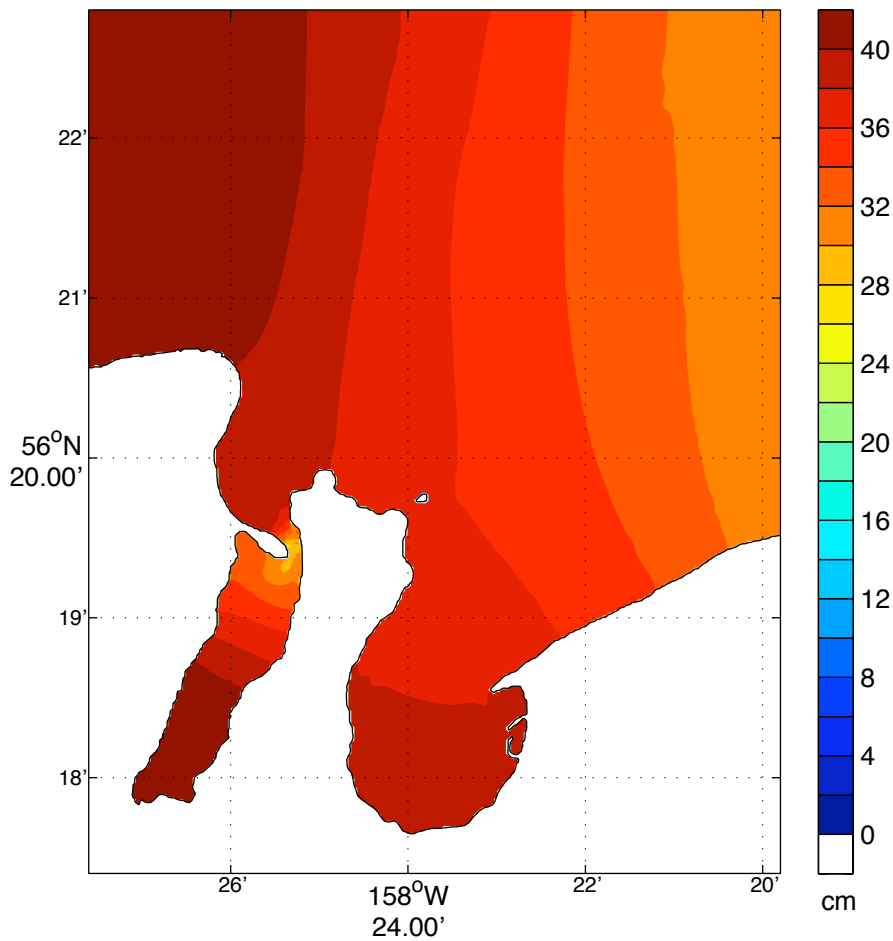

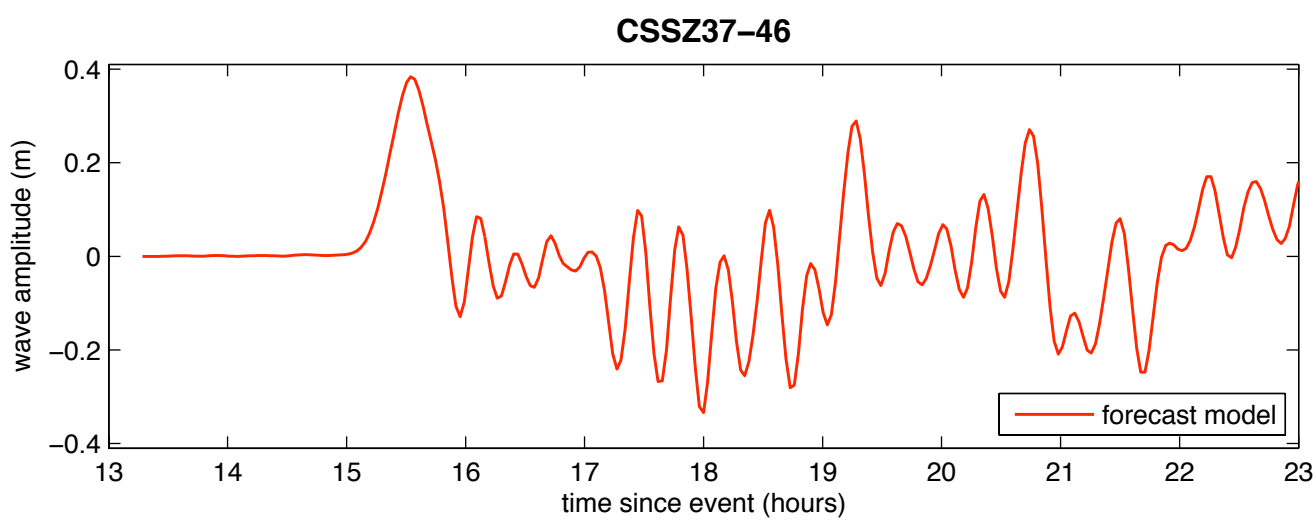

Figure 32 Results from the forecast model for the CSSZ 37-46 synthetic event. The upper panel shows the map of predicted maximum wave height in the Chignik C-grid and the lower panel shows the time series of wave amplitude at the warning point location.

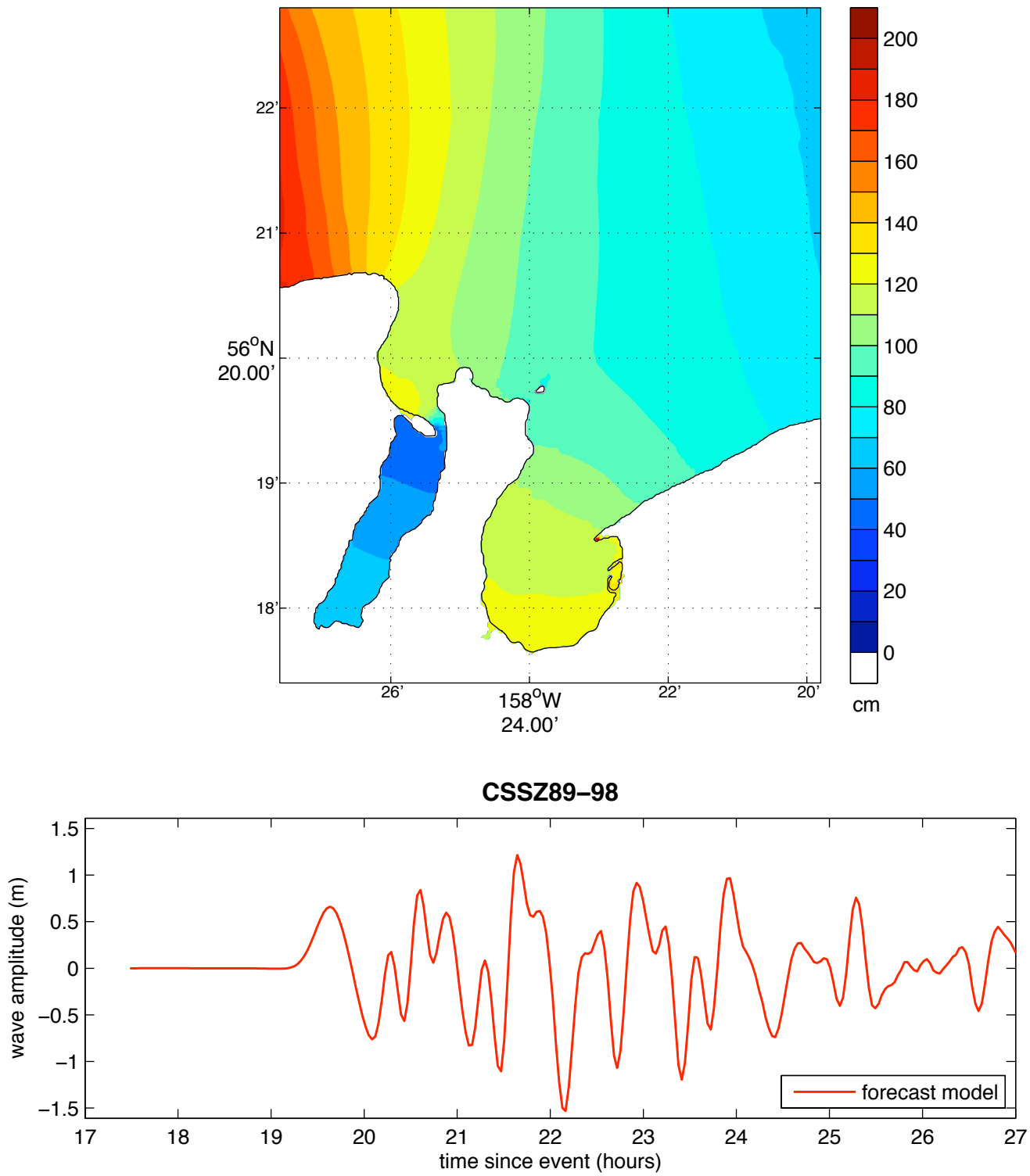

Figure 33 Results from the forecast model for the CSSZ 89-98 synthetic event. The upper panel shows the map of predicted maximum wave height in the Chignik C-grid and the lower panel shows the time series of wave amplitude at the warning point location.

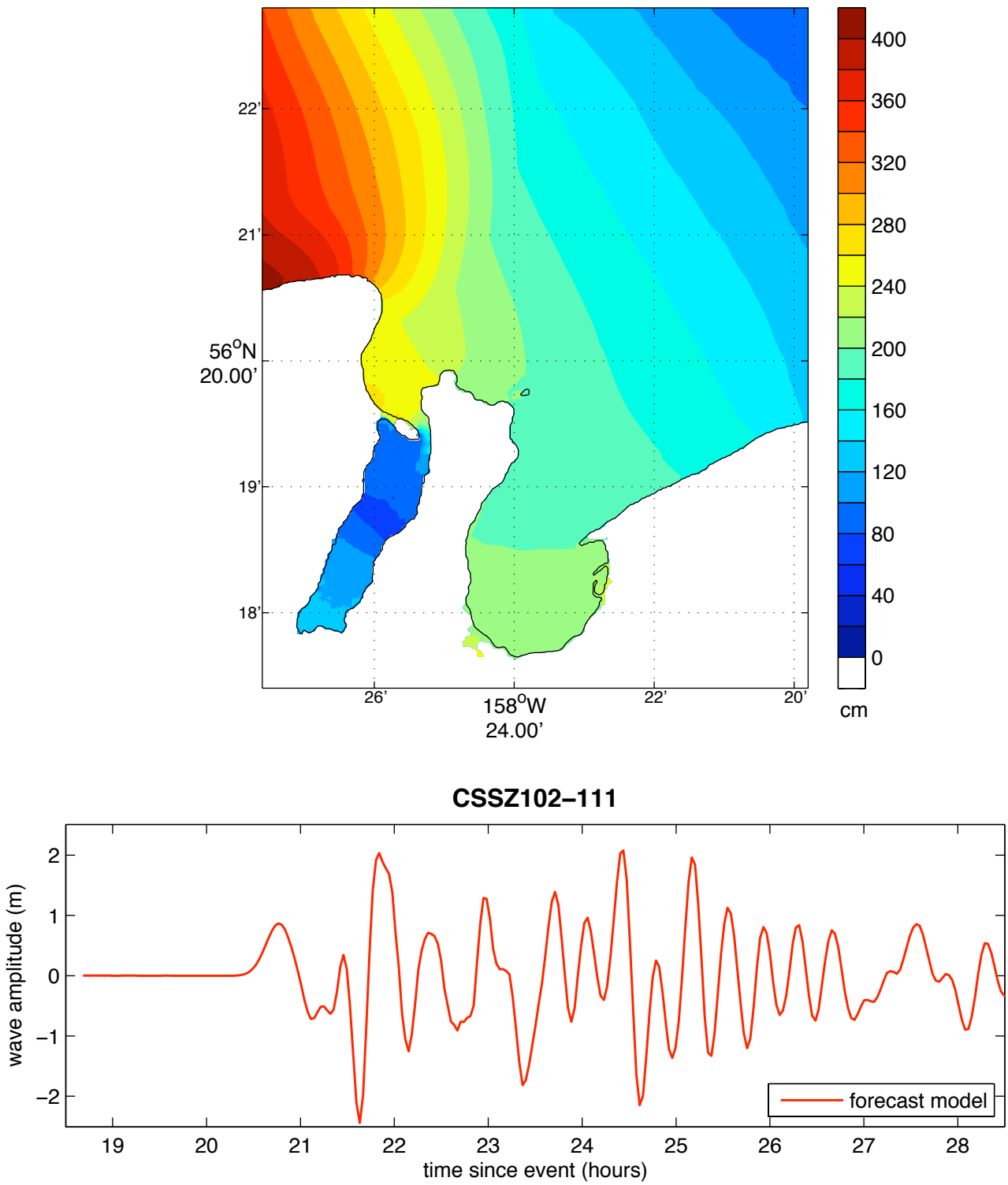

Figure 34 Results from the forecast model for the CSSZ 102-111 synthetic event. The upper panel shows the map of predicted maximum wave height in the Chignik C-grid and the lower panel shows the time series of wave amplitude at the warning point location.

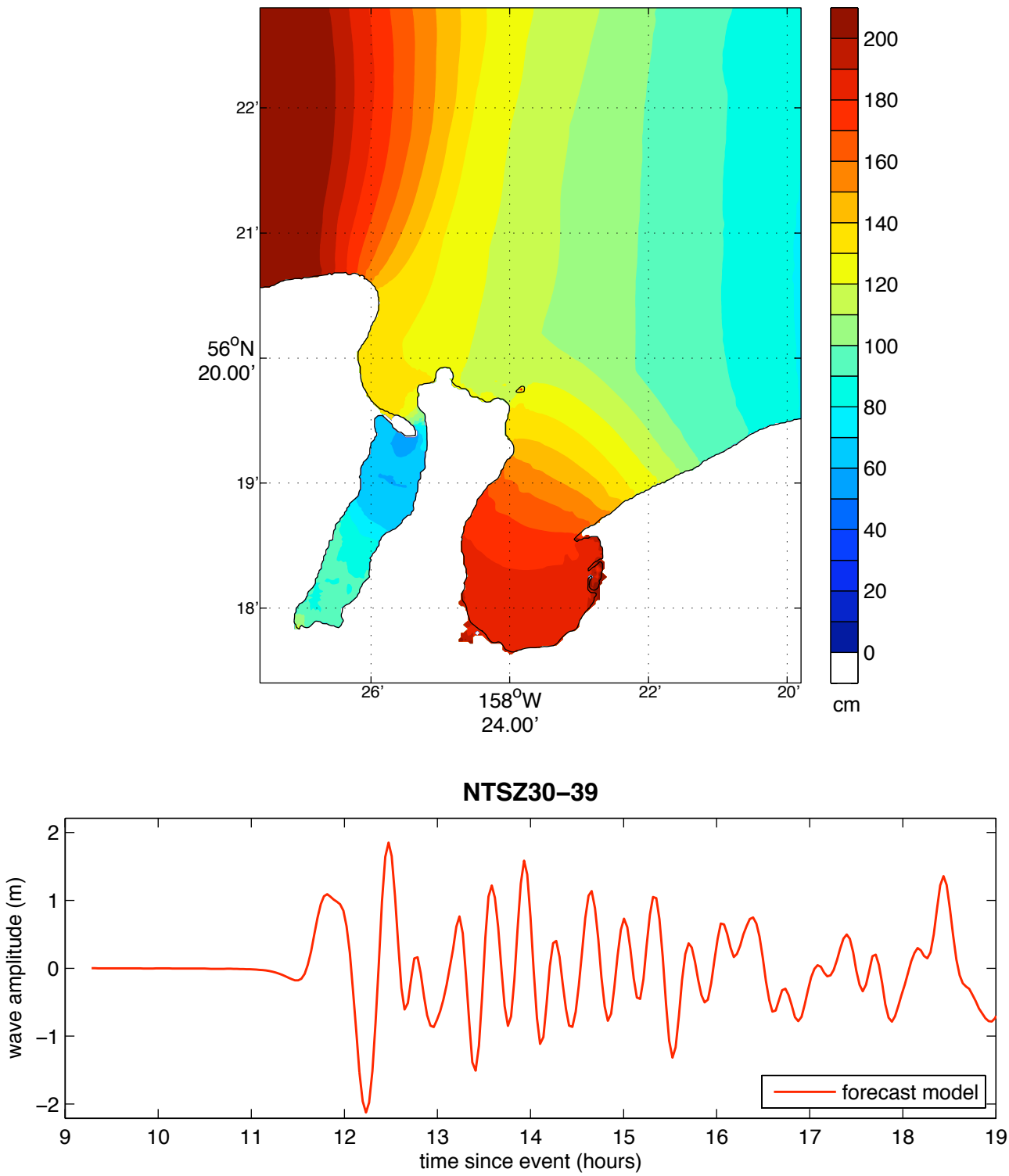

Figure 35 Results from the forecast model for the NTSZ 30-39 synthetic event. The upper panel shows the map of predicted maximum wave height in the Chignik C-grid and the lower panel shows the time series of wave amplitude at the warning point location.

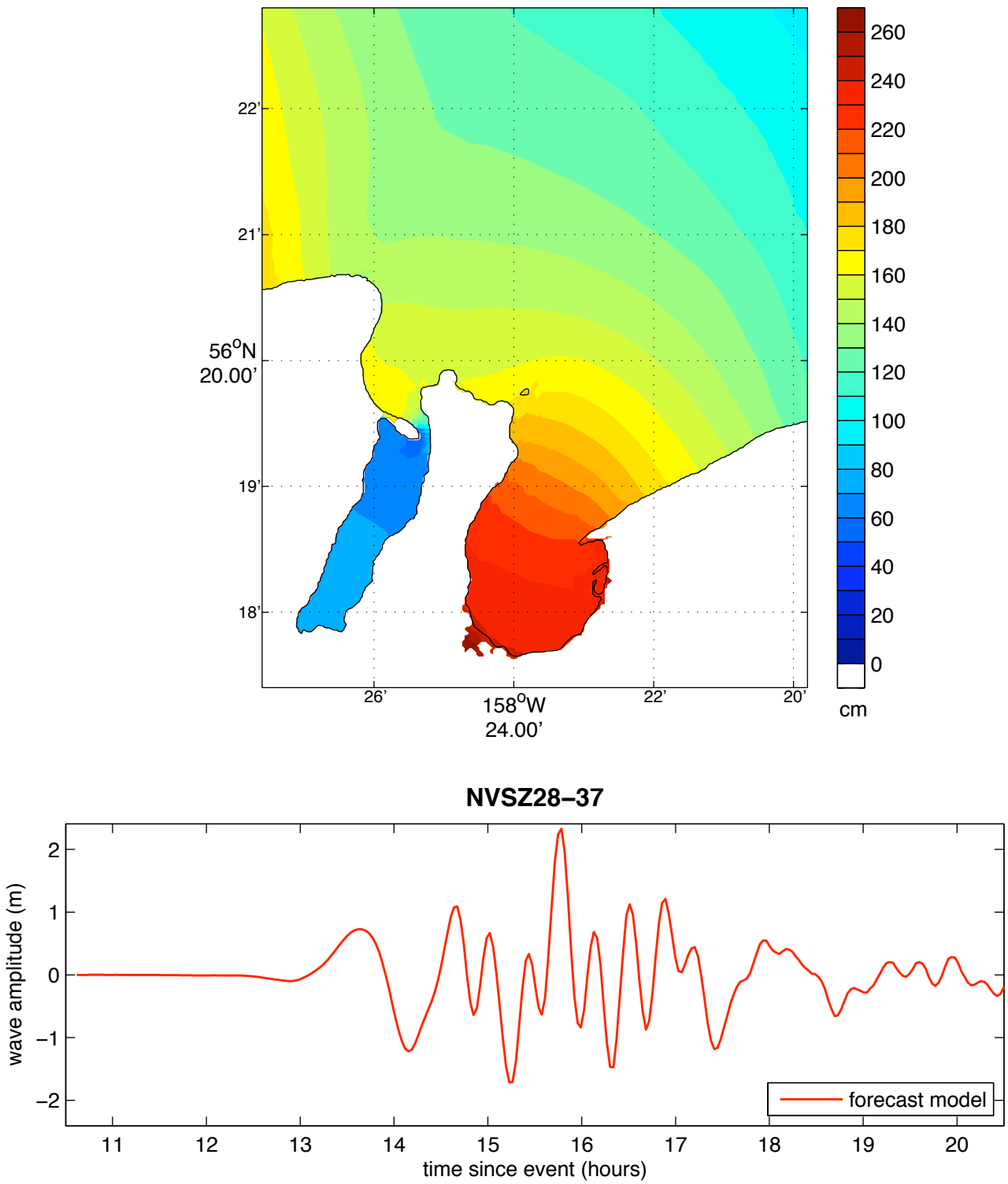

Figure 36 Results from the forecast model for the NVSZ 28-37 synthetic event. The upper panel shows the map of predicted maximum wave height in the Chignik C-grid and the lower panel shows the time series of wave amplitude at the warning point location.

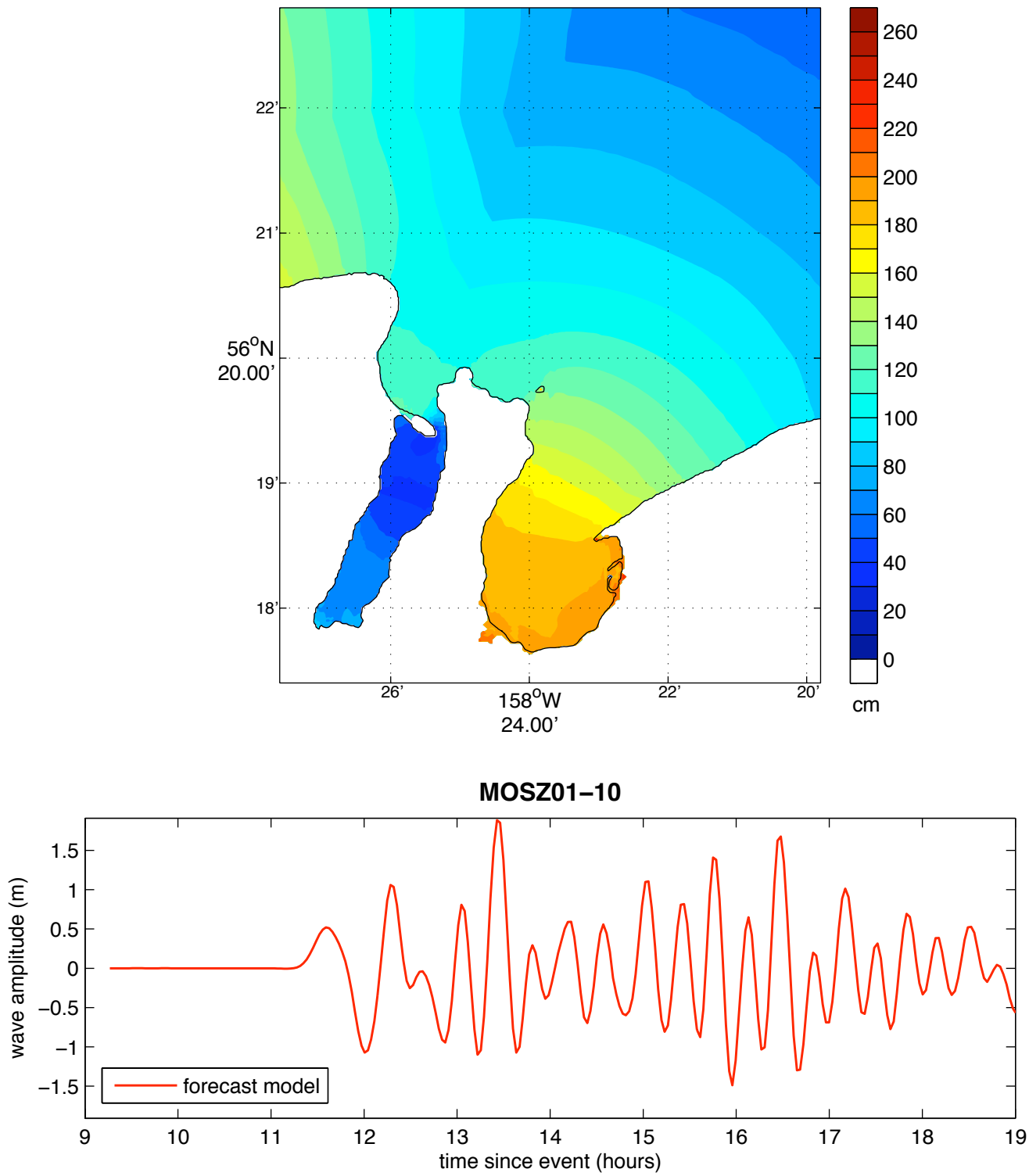

Figure 37 Results from the forecast model for the MOSZ 1-10 synthetic event. The upper panel shows the map of predicted maximum wave height in the Chignik C-grid and the lower panel shows the time series of wave amplitude at the warning point location.

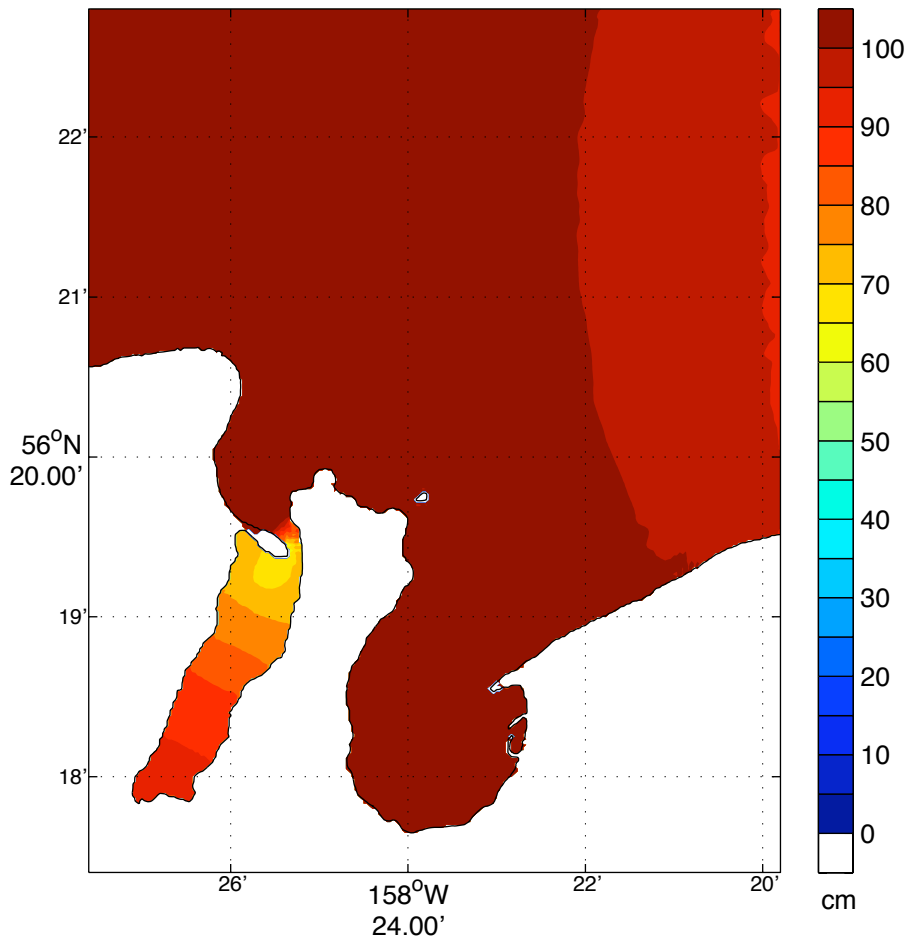

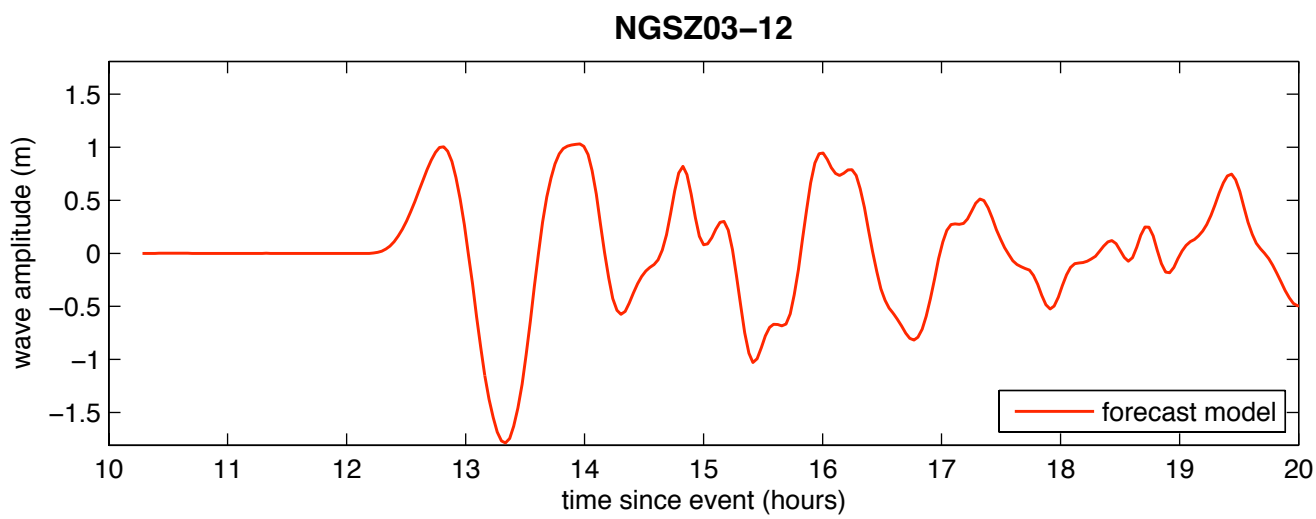

Figure 38 Results from the forecast model for the NGSZ 3-12 synthetic event. The upper panel shows the map of predicted maximum wave height in the Chignik C-grid and the lower panel shows the time series of wave amplitude at the warning point location.

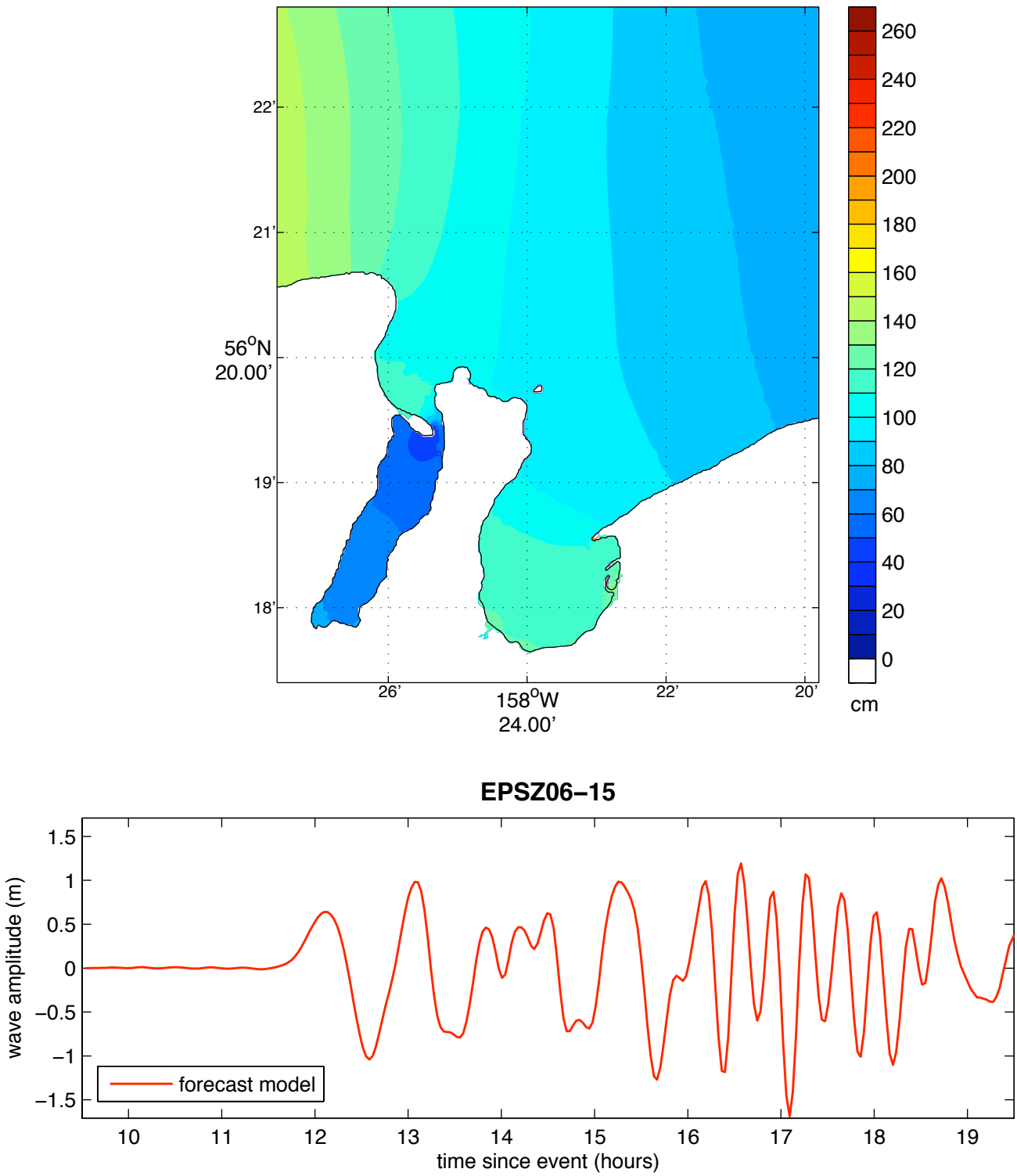

Figure 39 Results from the forecast model for the EPSZ 6-15 synthetic event. The upper panel shows the map of predicted maximum wave height in the Chignik C-grid and the lower panel shows the time series of wave amplitude at the warning point location.

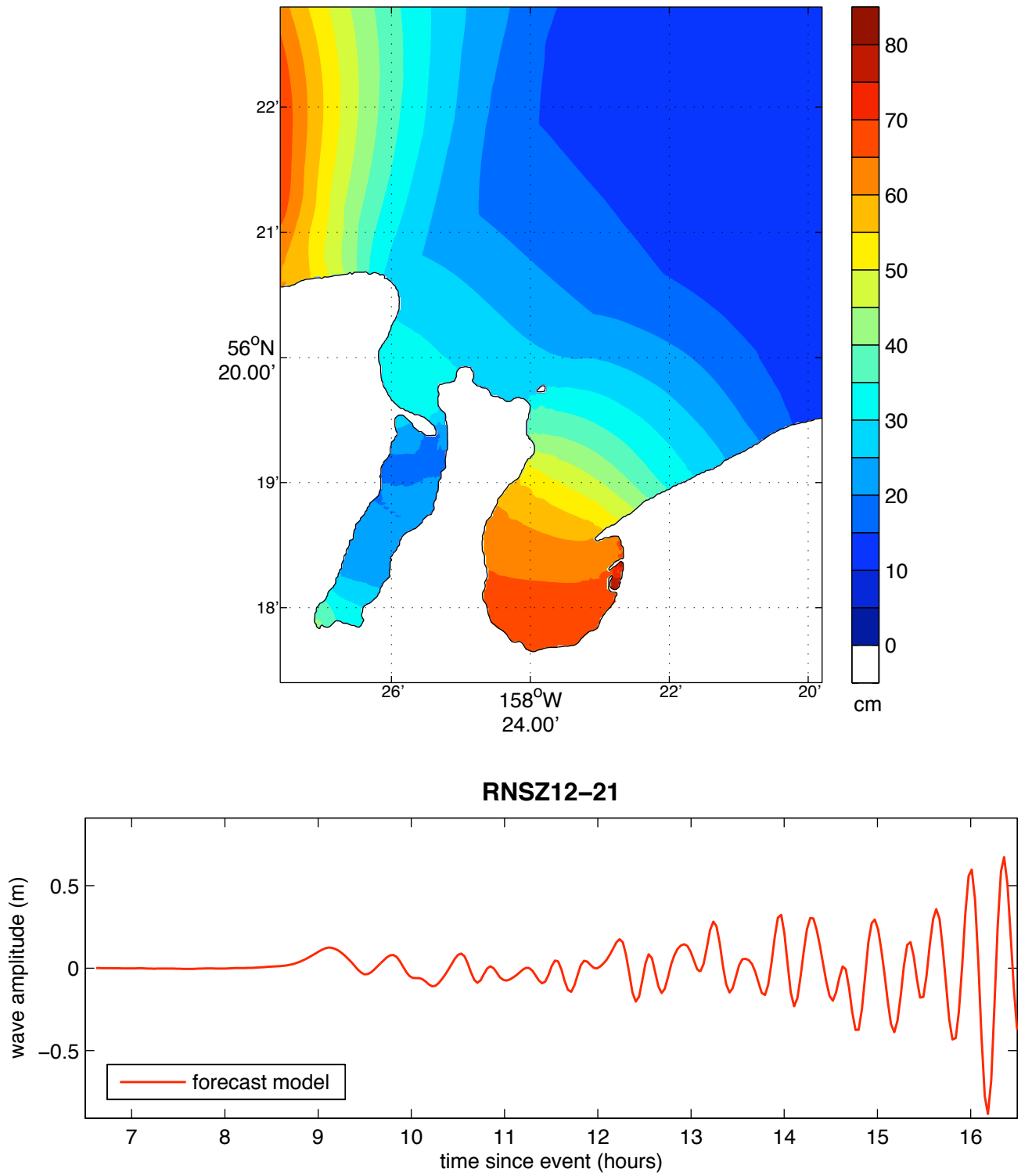

Figure 40 Results from the forecast model for the RNSZ 12-21 synthetic event. The upper panel shows the map of predicted maximum wave height in the Chignik C-grid and the lower panel shows the time series of wave amplitude at the warning point location.

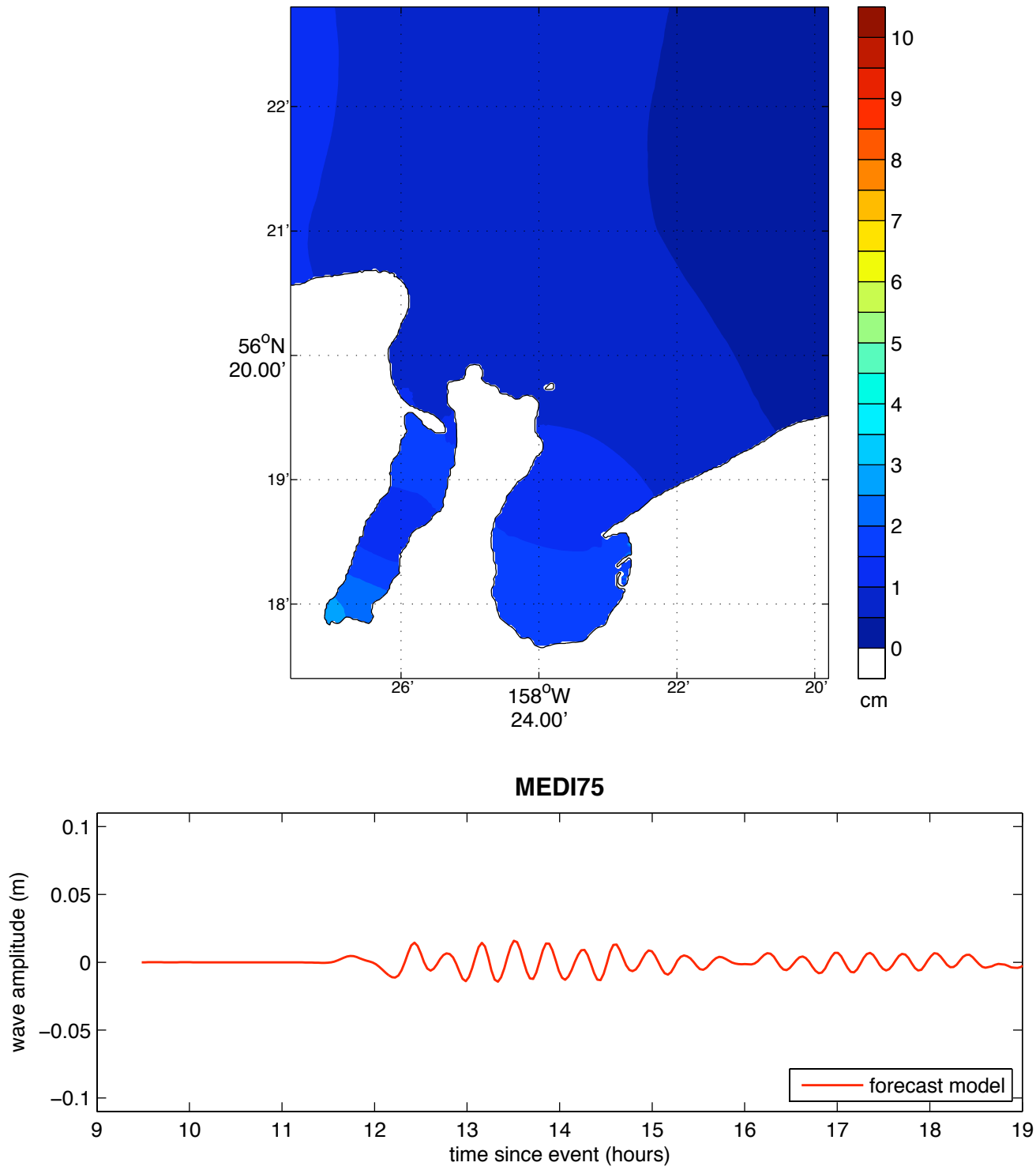

Figure 41 Results from the forecast model for the medium synthetic event, with a 1*NTSZb36 source. The upper panel shows the map of predicted maximum wave height in the Chignik C-grid and the lower panel shows the time series of wave amplitude at the warning point location.

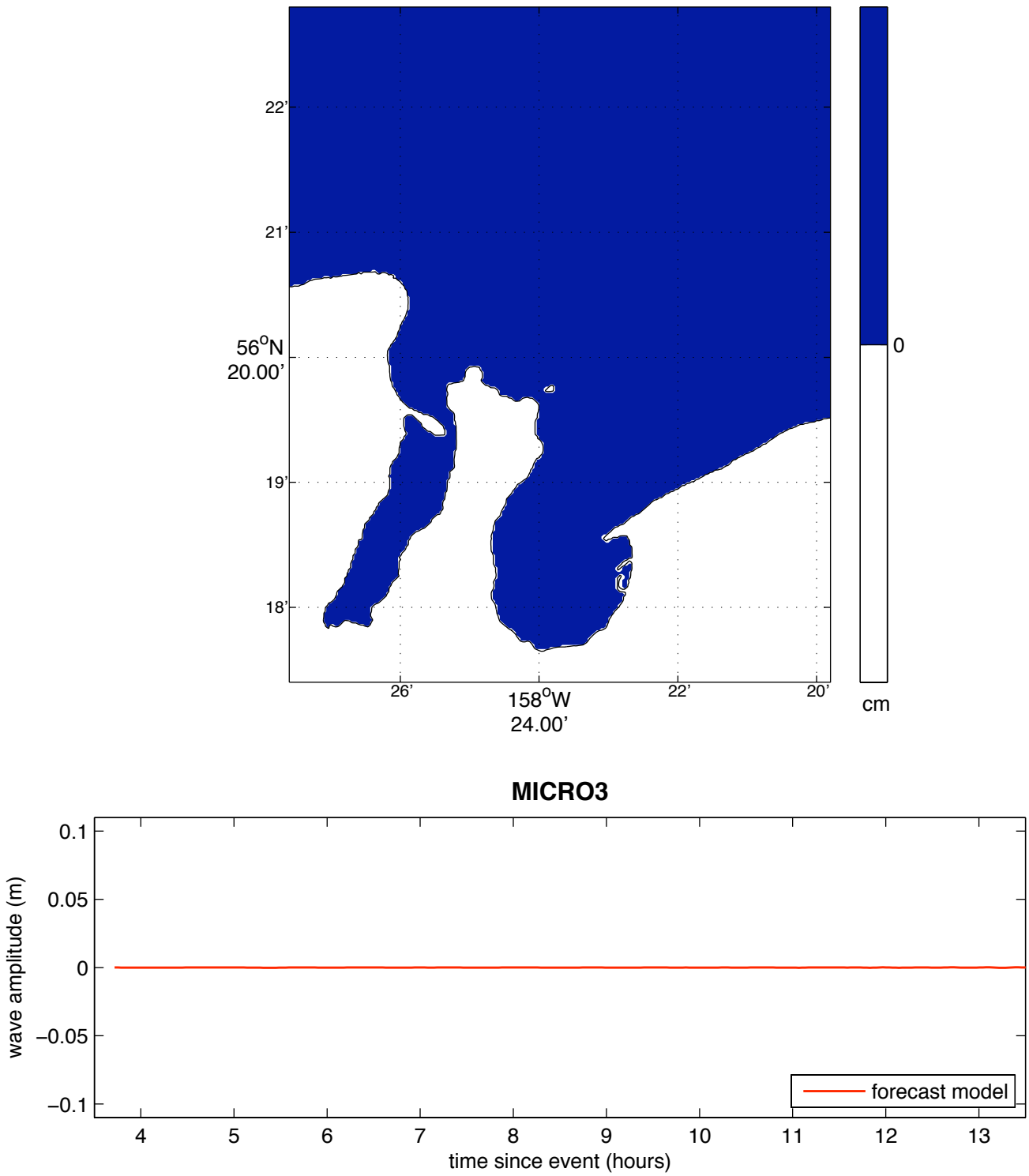

Figure 42 Results from the forecast model for the micro synthetic event which uses a source combination of 0.05*ACSZ b6. The upper panel shows the map of predicted maximum wave height in the Chignik C-grid and the lower panel shows the time series of wave amplitude at the warning point location.

Appendix A – should agree with table

A.1 Reference model *.in file

```
0.0001  Minimum amplitude of input offshore wave (m):
5       Input minimum depth for offshore (m)
0.1     Input "dry land" depth for inundation (m)
0.0009     Input friction coefficient (n**2)
1       let a and b run up
100.0    max eta before blow up (m)
0.25    Input time step (sec)
144000  Input amount of steps
12      Compute "A" arrays every n-th time step, n=
8       Compute "B" arrays every n-th time step, n=
408     Input number of steps between snapshots
0       ...Starting from
1       ...Saving grid every n-th node, n=
0000Template/chignikRA_2.most
0000Template/chignikRB_2.most
0000Template/chignikRC_2.most
```

A.2 Forecast Model *.in file

```
0.0001  Minimum amplitude of input offshore wave (m):
5       Input minimum depth for offshore (m)
0.1     Input "dry land" depth for inundation (m)
0.0009     Input friction coefficient (n**2)
1       let a and b run up
100.0    max eta before blow up (m)
0.8     Input time step (sec)
45000   Input amount of steps
6       Compute "A" arrays every n-th time step, n=
4       Compute "B" arrays every n-th time step, n=
156     Input number of steps between snapshots
0       ...Starting from
1       ...Saving grid every n-th node, n=
0000Template/chignikSA_2.most
0000Template/chignikSB_2.most
0000Template/chignikSC_8.most
```

Appendix B – Propagation data base